Hindawi
Adsorption Science & Technology
Volume 2023, Article ID 2018121, 21 pages
https://doi.org/10.1155/2023/2018121

Research Article

Adsorption of Arsenic, Lead, Cadmium, and Chromium Ions from Aqueous Solution Using a Protonated Chabazite: Preparation, Characterization, and Removal Mechanism

Laura Alejandra Pinedo-Torres,[1] Adrián Bonilla-Petriciolet,[2] María Elena García-Arreola,[3] Yenetzi Villagrana-Pacheco,[1] Ana G. Castañeda-Miranda,[4] and María Selene Berber-Mendoza[3]

[1]*Instituto Politécnico Nacional, Unidad Profesional Interdisciplinaria de Ingeniería Campus Zacatecas, Zacatecas 98160, Mexico*
[2]*Instituto Tecnológico de Aguascalientes, Aguascalientes 20256, Mexico*
[3]*Centro de Investigación y Estudios de Posgrado, Facultad de Ingeniería, Universidad Autónoma de San Luis Potosí, San Luis Potosí 78210, Mexico*
[4]*Programa en Ingeniería y Tecnología Aplicada, Laboratorio Nacional CONACYT, SEDEAM, Universidad Autónoma de Zacatecas, Zacatecas 9800, Mexico*

Correspondence should be addressed to María Selene Berber-Mendoza; selene.berber@uaslp.mx

Received 21 June 2022; Revised 1 October 2022; Accepted 6 October 2022; Published 25 January 2023

Academic Editor: Juan A. Cecilia

The adsorption of As(V), Pb(II), Cd(II), and Cr(III) ions from aqueous solutions on natural and modified chabazite was studied. The functionalization of chabazite was performed via a protonation and calcination with the aim of generating Lewis acid sites to improve its anion exchange properties. The surface and physicochemical properties of both adsorbents were studied and compared. The adsorption isotherms of tested heavy metal ions were quantified and modeled to identify the best isotherm equation. Steric parameters for the adsorption of these ions were also calculated with a monolayer statistical physics model. Natural chabazite showed the maximum adsorption capacity for Pb(II), while the modified zeolite improved its As(V) properties in 79%. These results showed that the modified zeolite was able to remove both cations and anions from aqueous solution. The application of this functionalized chabazite can be extended for the removal of other anionic pollutants from water, thus opening the possibility of preparing new adsorbents with tailored properties for water treatment.

1. Introduction

Heavy metal pollution is a relevant environmental problem worldwide due to its significant potential hazard to ecosystems and human health [1]. In particular, heavy metals dissolved in aqueous media are priority in terms of environmental protection because they are more toxic than the atomic form [2]. These soluble heavy metals include arsenic (As), lead (Pb), cadmium (Cd), and chromium (Cr), which are nonbiodegradable and have no physiological function. They have been reported as hazardous pollutants due to their toxicological profile, high solubility, environmental persistence, and accumulation into the food chain [3, 4]. Therefore, these dissolved heavy metals are classified as potentially toxic elements (PTEs).

According to the International Agency for Research on Cancer (IARC), these PTEs are also considered as carcinogenic [5] where their main exposure routes are the inhalation of contaminated air, skin absorption, and ingestion of polluted food or water [6–9]. Consequently, it is necessary to develop cost-effective and sustainable methods and materials to reduce the concentrations of these toxic species from polluted water and industrial effluents [10]. Nowadays, the adsorption is a simple and reliable technique for water and

wastewater treatment where its success mainly depends on the preparation of an effective adsorbent [11]. The most used adsorbents are activated carbons, zeolites, silica gel, activated alumina, and biochar [12–15].

Natural zeolites offer several advantages for water treatment. They are low-cost minerals present in various parts of the world, have pore sizes < 20 Å, and, consequently, are capable of adsorbing or rejecting molecules, which make them suitable as molecular sieves [16]. Zeolites also adjust the pH of the media, and their application usually does not generate additional environmental pollution [17].

In terms of chemical composition, zeolites are aluminosilicates with a structure consisting of a tetrahedral arrangement of silicon (Si^{4+}) and aluminum (Al^{3+}) cations with four oxygen anions (O^{2-}) at the vertices. This composition generates a three-dimensional framework containing SiO_4 and AlO_4 tetrahedral building blocks with permanent negative charges [18], which are balanced by monovalent or divalent counterions (e.g., alkaline or alkaline earth metals) that have the capability of acting as adsorption sites [19]. The adsorption process is controlled by the zeolite properties like ion exchange capacity and selectivity [20].

Chabazite is a zeolite used worldwide due its high surface area and physicochemical properties as ion exchanger [21–23]. Its framework has units of six double rings (D6R) interconnected through 4 rings, forming a 3-dimensional channel system that presents large ellipsoidal cavities with apertures consisting of 8 rings with a diameter of 3.8 Å in the cation-free condition [24, 25].

Natural chabazite can adsorb cationic species due to its negative charge. Different studies have reported the removal of different cations using this zeolite, thus obtaining a maximum adsorption capacity of 175 mg/g of Pb(II) [26]; 120 mg/g of Cd(II) [27]; 4.5 mg/g of Ni(II) [28]; 4.2–8.9 mg/g of Cu(II), Co(II), Zn(II), and Mg(II) [29]; and 30-45 mg/g of NH_4^+ [30, 31]. It has been established that its adsorption properties to remove cationic species in water treatment follow the next selectivity: $Cs^+ > NH_4^+ > K^+ > Pb^{2+} > Na^+ > Ba^{2+} > Cd^{2+} > Sr^{2+} > Cu^{2+} > Zn^{2+}$ [32].

On the other hand, the chabazite can be tailored via different processes to improve its adsorption performance for the removal of organic molecules and negatively charged species. For example, this material can be synthetized from urban wastes like cement and used to adsorb 129 mg/g of methylene blue [33]. This zeolite with the incorporation of copper was also able to adsorb NOx where the results showed that Cu-CHA catalysts prepared with a conventional wet ion exchange method outperformed the NOx conversion obtained with samples prepared via chemical vapor deposition and solid-state ion exchange [34]. A chemical treatment based on hexadecyltrimethylammonium bromide (HDTMA-Br) helped to change the external surface of this zeolite from negative to positive, thus being able to adsorb 26 mg/g of $Cr_2O_7^{2-}$ [35], 6.9 mg/g of AsO_4^{3-}, and 3.3 mg/g of PO_4^{3-} [36].

A straightforward modification process to improve the properties of zeolites relies on the decationation using different interchange ions like NH_4Cl, NaCl, or $Cu(NO_3)_2$ with the subsequent calcination at ≥450°C. This approach has been used to modify the surface properties of zeolites with the aim of removing anions in aqueous solution. Some examples are the removal of fluoride using clinoptilolite with a maximum adsorption capacity of 12.3 mg/g [37], the gasoline desulfurization employing 5A and 13X zeolites with a removal of 16.7 mg/g [38], and the nitrite removal from wastewater [39]. The superficial zeolite modification using NH_4Cl and a subsequent thermal treatment have been utilized to tailor synthetic chabazites for the thermal degradation of high-density polyethylene to low molecular mass hydrocarbons [40] and the adsorption of ethane (41 mg/g) and propane (81 mg/g) [41]. This material had been also employed as a catalyst in the methanol to olefins reaction (forming polyaromatic coke species) [42]. However, this approach has not been applied to improve the chabazite properties for the adsorption of anionic pollutants from water. Also, its impact on the cation adsorption properties of natural zeolites has not been analyzed in detail.

The aim of this study was to develop an effective and low-cost protocol to tailor the surface properties of the chabazite for the improvement of the adsorption of anionic species. This method was based on the decationation with NH_4Cl and protonation and subsequent calcination of natural chabazite. Results showed that this functionalization route was successful to generate Lewis acid sites (LAS) on this zeolite, thus increasing its anion adsorption properties. The performance of natural and modified zeolites was tested on the removal of As(V), Pb(II), Cd(II), and Cr(III) ions. The adsorption isotherms were correlated and analyzed with the Langmuir, Freundlich, Sips, Liu, and statistical physics models. The adsorption properties of these adsorbents were compared and correlated with their ion exchange capacity and chemical composition. The mechanisms of chabazite modification and adsorption of tested ions were analyzed. Finally, this study showed that the modified chabazite can be used to remove both anions and cations of water pollutants, thus being a promising approach for low-cost water depollution.

2. Methodology

2.1. Preparation of Modified Chabazite. Natural zeolite used in this study was obtained from a mineral deposit from the state of Sonora, Mexico. The natural chabazite (labelled as CH-N) was sieved to obtain a particle size < 125 μm, and these zeolite particles were utilized in the surface modification process, which was implemented according to a method adapted from Ghasemian et al. [43]. This method involved the following steps: (a) *Homogenization*: 50 g of zeolite was mixed with 500 mL of 2 N NaCl solution, stirred at 500 rpm and room temperature for 24 h [44]. Zeolite was washed several times with deionized water and dried at 100°C for 24 h. The sample obtained from the homogenization process was represented by the label "Z-Na". (b) *Decationation*: the dry zeolite was treated with ammonium chloride because the exchange of Na^+ is better for zeolites with NH_4^+ [45]. 12.5 g of homogenized chabazite was mixed with 250 mL of 1 N NH_4Cl at room temperature for 24 h under constant stirring. The final zeolite was washed with hot deionized water and dried at 100°C. The sample

obtained from the decationation process was labelled as "Z-NH_4^+". (c) *Thermal treatment*: decationated zeolite was calcined at 500°C for 3 h using a heating rate of 5°C/min. Then, the sample was washed with deionized water and dried at 100°C for 24 h. Finally, this modified zeolite (labelled as "CH-MS") was characterized and used for the adsorption experiments. Flow diagram of this process is included as Supplementary Information.

2.2. Chemical Characterization of Zeolite. The identification of the crystalline phases present in the zeolite samples was carried out by X-ray diffraction (XRD) analysis. XRD patterns were recorded with a diffractometer Siemens D5000 at room temperature. Samples were scanned within 2θ angular range of 5-50° with a step size of 0.020° for 10 s.

The textural parameters were determined by the Brunauer-Emmett-Teller method (BET) using a surface area and pore size analyzer (Quantachrome model nova 3200e). The samples were introduced into glass cell and degassed at 200°C for 10 h. N_2 physisorption was measured at -196.15°C.

The surface morphology of the zeolite samples was examined by using a scanning electron microscope (SEM) JEOL, model JSM-6610LV equipped with a microanalysis system model DX-4 energy dispersed spectroscopy (EDS). CH-N and CH-MS samples were placed on a fine coat brand carbon coater for this analysis.

Infrared spectra were obtained using Fourier transform infrared spectrophotometer (Thermo Scientific Nicolet iS10 FTIR). First, CH-N and CH-MS samples were dried at 70°C for 24 h to remove the moisture. Spectra of the samples were recorded in the region of 4000-600 cm^{-1}. FTIR analysis was also performed to determine the acid centers of tested adsorbents via the adsorption of pyridine. Samples of CH-N and CH-MS were subjected to vacuum and then exposed to pyridine atmosphere for 24 h. FTIR spectra of pyridine-loaded samples were recorded and analyzed.

The thermogravimetric analysis (TGA) was done using a PerkinElmer equipment (model Pyris Diamond TGA/DTG) calibrated with indium and gold samples from 25 to 660°C and 1063°C, respectively. 0.2 mg of zeolite sample was analyzed in the temperature range of 25–700°C with increments of 10°C/min.

The procedure established by Corbin et al. [46] was utilized for the determination of chemical composition of CH-N and CH-MS. The samples were sieved to obtain a particle size of 0.18 mm, and then, 0.1 g was mixed with 0.2 g of $LiBO_2$ and 0.4 g of $Li_2B_4O_7$. The mixtures were placed in a graphite crucible with a drop of LiBr (25%w/w) and calcined for 30 min at 900°C in a muffle. The melted mixture was dissolved in 75 mL of HNO_3 (10%w/w), filtered and made up to 200 mL. The concentrations of dissolved metals were quantified with a Thermo Scientific Inductively Coupled Plasma Optical Emission Spectrometry (ICP-OES). Multielement solutions containing Fe, Mn, Ca, Mg, K, Si, Na, Al, Sr, Pb, Sn, Hg, Cd, Zn, As, Ni, Cr, Mo, and Ba were used to prepare the calibration curve where high purity standard solutions (1000 mg/L) of each metal and deionized water were employed for this purpose.

2.3. Surface Properties of Zeolites. The pH of the point of zero charge (PZ) of the zeolites was determined preparing solutions with pH between 2.27 and 6.75 (with a constant ionic strength of 0.01 M) via the mixing of certain volumes of 0.01 M NaOH, HNO_3, and $NaNO_3$ with 0.005 g of the samples at 25°C under constant stirring of 30 rpm for 5 days in an orbital shaker. Finally, the zeta potential of the zeolite particles was obtained using the zetameter (Zetasizer, Malvern model Nano series).

Cation exchange capacity (CEC) was obtained using a methodology reported by Ming & Dixon [47] where 1 g of CH-N and CH-MS samples was saturated with Na^+ ions (using 50 mL of 1 N $C_2H_3NaO_2$ for 24 h) and washed, and the exchange of Na^+ ions for NH_4^+ ions was done using 50 mL of 1 N $C_2H_7NO_2$ at room temperature for 24 h. Na^+ ion concentration was measured with an ICP-OES, and the CEC (meEq/g) was determined with the following equation:

$$\mathrm{CIC}\left(\frac{\mathrm{mEq}}{100\mathrm{g}}\right) = \frac{[\mathrm{Na}^+]\, V.100}{m\,\mathrm{MW}}, \tag{1}$$

where $[\mathrm{Na}+]$ is the Na^+ concentration (mg/L), V is the volume (L), m is the mass of chabazite (g), and MW is the Na^+ molecular weight (mg/mEq).

2.4. Adsorption Studies Using Zeolites. Adsorption studies were conducted with both zeolites CH-N and CH-MS in glass Erlenmeyer flasks containing 0.05 g of the adsorbent and 0.040 L of the pollutant solution. These studies were performed at pH 4 where the solution pH was adjusted by adding HNO_3 or NaOH and mixing with a glass stirrer. Note that this solution pH was selected to avoid the precipitation of Cd(II) and Pb(II) ions as hydroxides (i.e., $Cd(OH)_2$ and $Pb(OH)_2$ at pH > 5 and 6, respectively) [48, 49] and to prevent the zeolite dealumination [31, 50]. Other studies have also reported that a maximum adsorption capacity of Pb(II), Cd(II), and Cr(III) ions can be obtained with different adsorbents at pH 4 [48, 51, 52]. Initial concentrations of 1-59, 20-500, 10-112, and 5-93 mg/L for As(V), Pb(II), Cd(II), and Cr(III), respectively, were used in the adsorption experiments. These solutions were prepared with J.T. Baker standard solution of 1000 mg/L of each metal and deionized water. The suspensions (adsorbent+pollutant solution) were stirring at 50 rpm and $25 \pm 0.5 \circ$C in a thermoregulated orbital shaker (IKA model KS 4000) for 5 days. This time was enough to reach the equilibrium according to preliminary adsorption experiments at tested conditions. The quantification of metal concentrations was done using ICP-OES. The calibration curve for the quantification of these metals was obtained with solutions that were prepared using a high purity standard solution (1000 mg/L) of each adsorbate and deionized water. The removal of ions per unit mass of adsorbent (i.e., adsorption capacity) was expressed as q_e (mEq/g) and calculated with the mass balance given by the following equation:

$$q_e = \frac{V}{m}(C_o - C_e), \tag{2}$$

where C_o and C_e are the initial and equilibrium concentrations (mEq/L) of tested ion in the aqueous solution. Finally, the speciation of tested heavy metals was obtained by means of Hydra-Medusa speciation software at pH 0–14 and 25°C.

2.5. Isotherm Modeling. The experimental equilibrium data were modeled to analyze As(V), Pb(II), Cd(II), and Cr(III) adsorption and to explain the interactions of these heavy metal ions with CH-N and CH-MS samples. The best isotherm model for the removal of these pollutants was also identified. Therefore, four different isotherm models were tested using a nonlinear regression procedure. They corresponded to two-parameter (Langmuir and Freundlich) and three-parameter (Liu and Sips) isotherm models.

Langmuir is a monolayer adsorption model where the adsorbent saturation occurs assuming active sites with the same energy. This model considers that there is only one interaction corresponding to one active site per specie, and this isotherm is presented in equation (3) [53]. Freundlich is a multilayer adsorption model where the energy of active sites is not homogeneous, and this model is commonly applied to analyze heterogeneous systems. This isotherm model is presented in equation (4) [54]. Alternatively, Sips model can be reduced to the Freundlich and Langmuir models at low and high concentrations, respectively, and it presents the advantages of these two models since it is a combination of them. This isotherm model is given by equation (5) [55]. The Liu isotherm is a Langmuir-Freundlich type isotherm that has the advantage over the Sips model because its exponent has no restrictions in terms of its maximum value where it is >0. This isotherm is presented in equation (6) [56]. In summary, the corresponding equations of these isotherm models are given by

$$q_e = \frac{q_L K_L C_e}{1 + K_L C_e}, \tag{3}$$

$$q_e = K_F C_e^{\,1/n_F}, \tag{4}$$

$$q_e = \frac{q_S K_S C_e^{n_S}}{1 + K_S C_e^{n_S}}, \tag{5}$$

$$q_e = \frac{q_{LF}(K_{LF}Ce)^n LF}{1 + (K_{LF}Ce)^n LF}, \tag{6}$$

where q_L, q_S, and q_{LF} are the maximum adsorption capacities of the Langmuir, Sips, and Liu equations (mEq/g); K_L, K_S, K_{LF}, and K_F are the constants of the Langmuir, Sips, Liu (L/mEq), and Freundlich $(\text{mEq/g})(\text{L/mEq})^{1/\text{nF}}$ isotherms; and n_F, n_S, and n_{LF} are the dimensionless exponents (parameters related to the adsorption intensity that represents the relative distribution of the heterogeneity and the energy of the adsorption sites) of the Freundlich, Sips, and Liu equations, respectively.

A nonlinear least squares method based on an optimization algorithm was used to obtain the isotherm model parameters. The Solver tool of Microsoft Excel software was used to minimize the sum of the square error (ERRSQ) [57]:

$$(\text{ERRSQ}):\ \sum_{i=1}^{N} \left(q_{t,\text{meas}} - q_{t,\text{calc}}\right)_i^2, \tag{7}$$

where $q_{t,\text{meas}}$ is the adsorption capacity from the experiment (mEq/g), $q_{t,\text{calc}}$ is the adsorption capacity calculated with the isotherm model (mEq/g), and N is number of experimental points.

To compare and assess the performance of the isotherm models, three statistical metrics were calculated: determination coefficient (R^2), the average percentage deviation (%D), and chi-square (X^2) [57–59]. These metrics are given by the following equations:

$$R^2 = \frac{\sum_{i=1}^{N}\left(q_{t,\text{calc}} - \overline{q_{t,\text{meas}}}\right)^2}{\sum_{i=1}^{N}\left(q_{t,\text{calc}} - \overline{q_{t,\text{meas}}}\right)^2 + \sum_{i=1}^{N}\left(q_{t,\text{calc}} - q_{t,\text{meas}}\right)^2}, \tag{8}$$

$$\%D = \left[\frac{1}{N}\sum_{i=1}^{N}\left|\frac{q_{t,\text{meas}} - q_{t,\text{calc}}}{q_{t,\text{meas}}}\right|\right].100\%, \tag{9}$$

$$X^2 = \sum_{I=1}^{i=N} \frac{\left(q_{t,\text{meas}} - q_{t,\text{calc}}\right)^2}{q_{t,\text{calc}}}. \tag{10}$$

A monolayer adsorption model [60] was also utilized in the isotherm data correlation with the aim of analyzing the main steric parameters involved in the removal of these ions. This model was defined by

$$q_e = \frac{n_{\text{ads}} N_{\text{zeolite}}}{1 + \left(C_{\text{med}}/C_e\right)^{n_{\text{ads}}}}, \tag{11}$$

where n_{ads} is the number of ions adsorbed per functional group of zeolite, N_{zeolite} (mEq/g) is the quantity of zeolite functional groups involved in the adsorption of these pollutants, and C_{med} (mEq/L) is the adsorbate concentration at the half saturation condition, respectively.

3. Results and Discussion

3.1. Surface Chemistry Characterization of CH-N and CH-MS. Figure 1 shows the X-ray diffraction patterns of both zeolites used in this study. For CH-N, it was possible to confirm the presence of the expected chabazite structure characterized by its main peaks at 9.39° (1 0 1), 20.43° (-2 1 0), and 30.37° (-3 1 1) according to the JCPDS card 34-137 [61]. This result also agreed with the calculated XRD patterns reported for this zeolite [62]. X-ray diffraction pattern of CH-MS indicated that the crystalline structure remained after the modification process, thus preserving all the intensity peaks similar to CH-N. These findings could suggest that the modification took place only on the external surface, which agreed with the previous studies [63, 64]. Additionally, it was possible to observe an increase in the intensity of the peaks in the modified zeolite. This observation agreed with other studies (e.g., [37]) where an increment of the

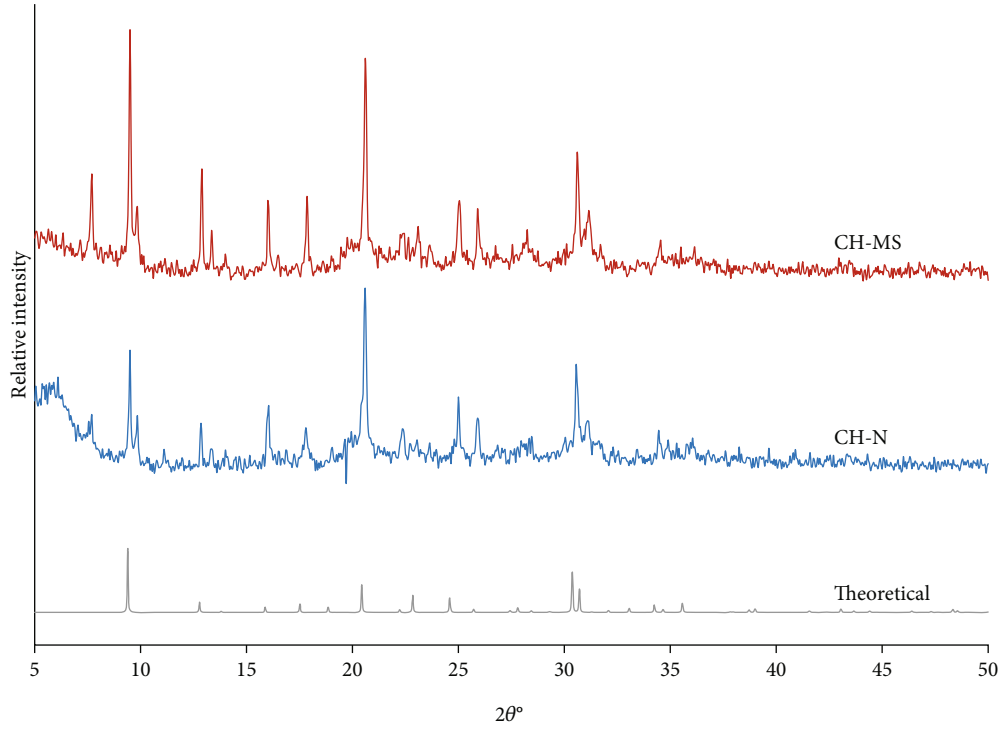

Figure 1: X-ray diffraction patterns of CH-N and CH-MS. Label "Theoretical" corresponds to the calculated pattern from International Zeolite Association, which was used as a reference pattern.

Table 1: Textural properties of CH-N and CH-MS samples.

Zeolite	Surface area (m^2/g)	Pore diameter (nm)	Pore volume (cm^3/g)
CH-N	324.2	2.94	0.198
CH-MS	325.9	3.04	0.216

intensity after a similar modification to a natural zeolite was also identified.

The textural properties of CH-N and CH-MS are given in Table 1. According to these results, CH-N surface area (324.4 m^2/g) was higher than some values reported in the literature for natural zeolites such as 2.7 m^2/g for perlite consisting of zeolites X (FAU type), P (GIS type), and phillipsite [65]; 20.3, 42, and 258 m^2/g for clinoptilolite [66–68]; 68 and 305 m^2/g for modernite [68, 69]; and 202 m^2/g for a natural chabazite from Mexico [31]. However, this value was lower than 1100 m^2/g of a natural chabazite supplied by Minerals Research-Clarkson, NY, USA [70].

Regarding the texture properties of CH-N and CH-MS, the differences between their surface areas and pore diameters were 0.52% and 3.35%, which were not significant because they were within the error interval of the equipment used in sample analysis. Nevertheless, the difference in pore volume corresponded to an increment of 8.33% that was statistically significant. It is convenient to remark that the behavior of the texture properties of different zeolites submitted to the similar surface modification treatment has been associated to the changes on their micropore structure. Both increments and reductions in these textural parameters have been reported. For instance, Saucedo-Delgado et al. [37] reported an increment of 90.6 and 22% in the surface area and pore volume of clinoptilolite. On the other hand, Albayati and Kalash [71] proved that the functionalization (via the reaction between the silylating agent and the silanol groups) of mesoporous silica MCM-41 incremented the surface area from 28.7 to 300 m^2/g, while the calcined MCM-41 showed the highest surface area (i.e., 1000 m^2/g). In the contrary case, a decrease of 15.5 and 23% in pore diameter and surface area of modernite was reported by Mori et al. [72], while Atiyah et al. [73] obtained surface areas of 845 and 45 m^2/g for the mesoporous silica SBA-15 and its functionalized form NH_2/SBA-15, respectively, thus indicating a significant decrement of this textural parameter.

SEM micrographs of chabazites showed the typical rhombohedral crystals that were consistent with the previous studies [31, 74, 75]. By comparing these micrographs, it was possible to observe that CH-N (Figure 2(a)) presented a well-defined structure, while CH-MS (Figure 2(b)) showed partially formed rhombohedral structures. This could be explained because during the modification process, the minerals were washed several times, which could fragment the zeolite agglomerates. Chemical analysis of CH-N crystals by SEM-EDX (Figure 2(a)) indicated the presence of the characteristic elements of zeolites: Si, Al, O, Mg, Ca, K, and Na. On the other hand, EDX results showed that the exchangeable cations (Na^+ and Ca^+) of CH-MS (Figure 2(b)) were expelled out from the framework, where this effect agreed with the result obtained by Barrer et al. [76] and Ghasemian et al. [43]. This behavior can be explained by the fact that, during the homogenization phase carried out for chabazite, Na^+ displaced the majority of Ca^{2+}. Then, the sodium ions were exchanged with

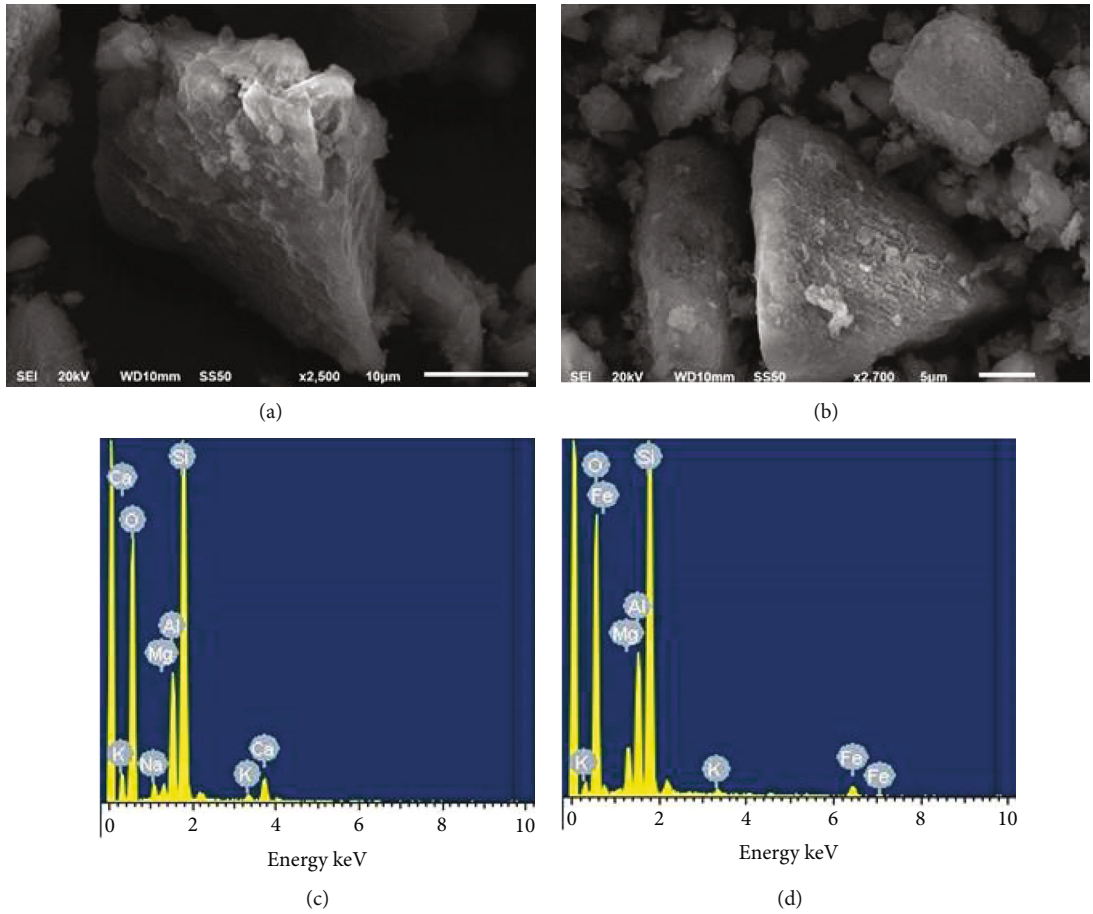

Figure 2: (a, b) SEM micrographs and (c, d) SEM/EDX elemental microanalysis for CH-N and CH-MS samples.

the ammonium ions when the zeolite was treated with NH_4Cl because the thermodynamic affinities for the exchange reactions in chabazite followed the next sequence: $NH_4^+ > Na^+ > Ca^{2+}$, which were given by the standard free energies of exchange [76].

Figure 3(a) presents the FTIR spectra of CH-N and CH-MS at 4000-600 cm^{-1}. At 750–650 and 1250–950 cm^{-1}, these spectra displayed the internal vibrations of TO_4 tetrahedron (T = Si and Al) named as OH stretching (indicated by the four-membered ring structure) and asymmetry stretching. The absorption band between 570 and 635 cm^{-1} indicated 6-membered rings. The external vibrations of the tetrahedron (i.e., T–O double ring, symmetry and asymmetry stretching) appeared at 650-500, 820-750, and 1150-1050 cm^{-1}, respectively [77]. The absorption bands observed at 1640, 3600, and 3380 cm^{-1} were characteristic to the water bending vibration, isolated, and H-bonded hydroxyl groups, respectively [78]. These three bands for CH-N sample showed higher intensities than those observed for CH-MS, thus indicating that CH-N had a higher water content that was lost in the modified zeolite upon calcination. Another major difference was that CH-MS sample showed an absorption band at 3640 cm^{-1} corresponding to the hydroxyl group formed during the modification process [79]. Both types of vicinal hydroxyl groups were observed via the bands at 3640 and 3700–3740 cm^{-1} that was associated to the silanol nests [80].

It was possible to observe that CH-MS did not present the characteristic bands of NH_4^+ form (i.e., the Lewis bond NH_3 at 1630 cm^{-1}, while NH_4^+ is characterized by bands between 1400 and 1500 cm^{-1} and NH stretching frequencies at 3800 cm^{-1}) because they disappeared due to the heating at 290°C [81].

Figure 3(b) reports the FTIR spectra of CH-N and CH-MS samples loaded with pyridine at 1400-1700 cm^{-1}. The absorption bands at 1640 and 1545 cm^{-1} have been attributed to the pyridine adsorption and were characteristic of the Brönsted acid sites (BAS). The bands located at ~1430 and 1490 cm^{-1} corresponded to hydrogen-bonded pyridine (H-pyridine), while the bands identified at 1590 and 1450 cm^{-1} have been attributed to coordinately bound pyridine, thus being an indicator of Lewis acidity [82–84]. The intensity of the absorption bands of LAS (1450 and 1590 cm^{-1}) and BAS (1640 cm^{-1}) in the spectrum of pyridine-loaded CH-MS were higher than those of the other zeolite sample. This was due to the modification where BAS and LAS sites were formed. Emeis [85] reported similar results where pyridine adsorption was studied for natural and calcined modernite at 550°C for 2 h. Other studies of Ward [86] showed an infrared spectrum of pyridine adsorbed on a rare earth Y zeolite calcined at 430 and 680°C, while Wu and Weitz [87] reported the results for a ZSM-5 zeolite modified (protonated with nitrate salt and calcined at 500°C).

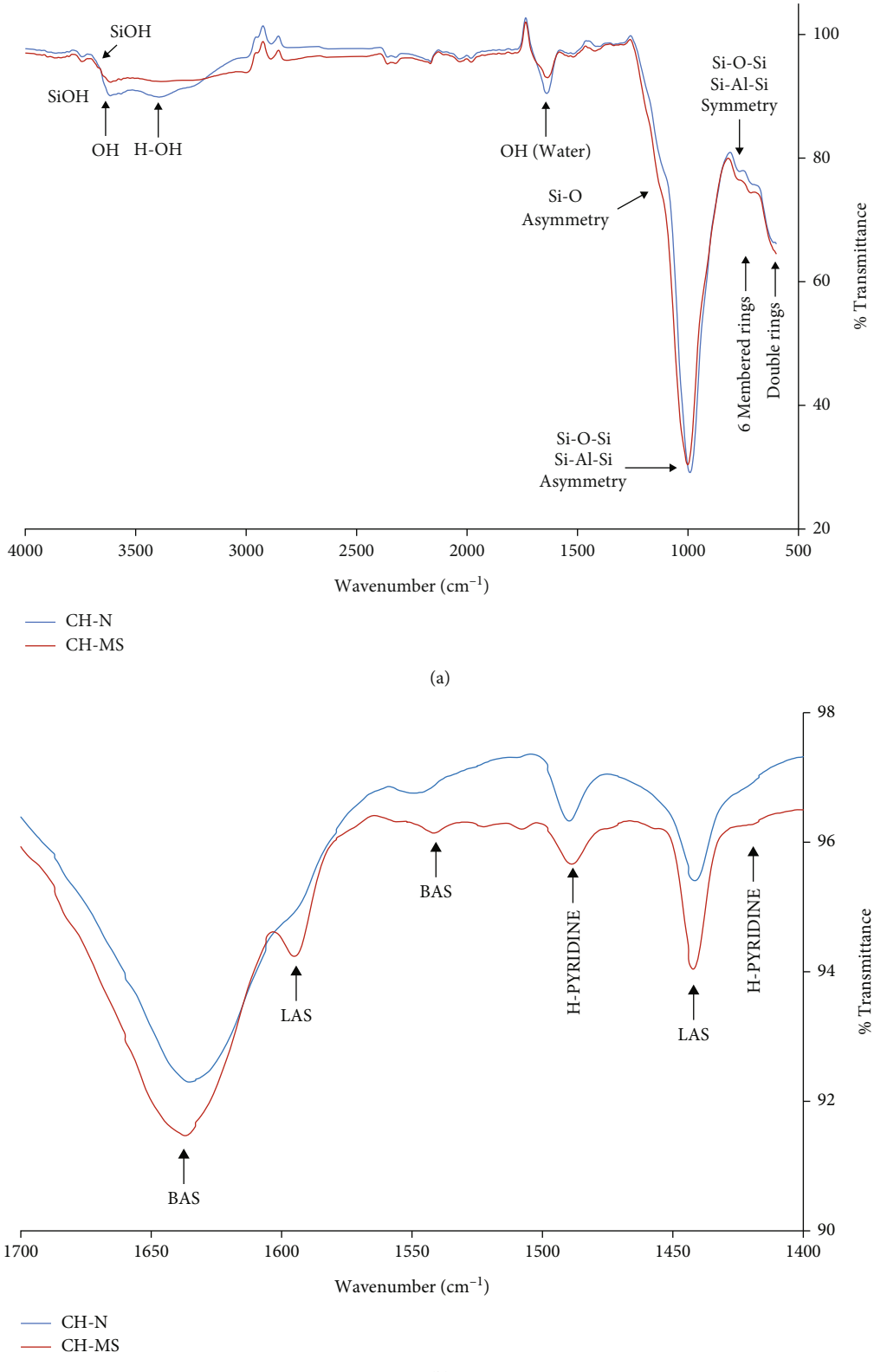

Figure 3: FTIR spectra of CH-N and CH-MS samples (a) without and (b) with loaded pyridine.

Figures 4(a) and 4(b) show the thermogravimetric (TGA) and differential (DTG) analysis curves for CH-N and CH-MS samples. TGA results indicated that the weight of both samples decreased considerably with the increase of temperature up to ~600°C. Then, there was a slow and progressive weight reduction. The weight loss was 16.55% for

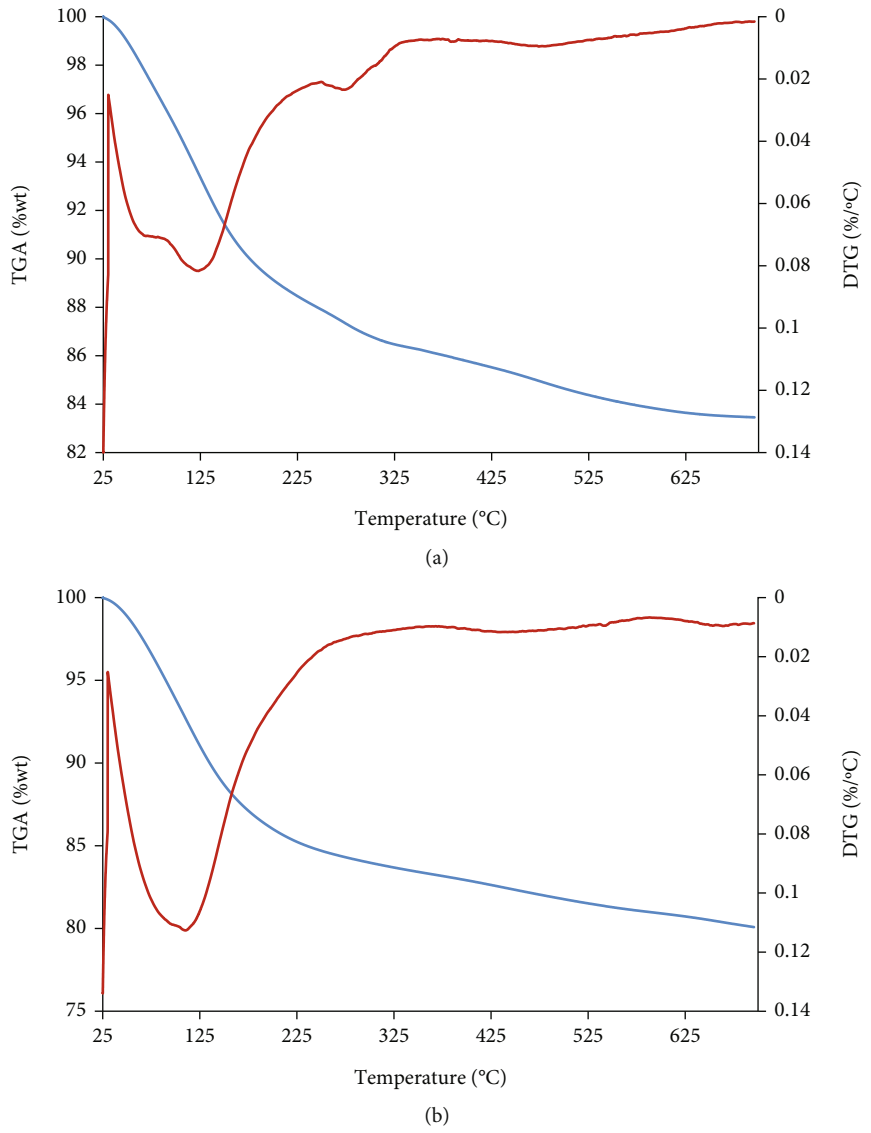

Figure 4: Results of TGA and DTG for the zeolite samples: (a) CH-N and (b) CH-MS.

Table 2: Chemical composition of the chabazite and its modified form.

Zeolite	wt%								Si/Al ratio
	Fe	Ca	Mg	K	Si	Na	Al	Others	
CH-N	3.76	5.95	4.31	3.12	60.11	3.65	18.22	0.88	3.3
CH-MS	3.75	0.00	3.98	3.00	64.65	0.00	24.10	0.52	2.8

CH-N and 19.92% for CH-MS. DTG curve showed the water loss from CH-N sample in two steps. The first step at 81°C was attributed to the humidity loss of the zeolite, while the second step at 118°C corresponded to the loss of structural water from the zeolite. The decomposition of calcium carbonate was associated to the peak at 270°C, which was consistent with the study of Stakebake [88] that indicated that this phenomenon could occur before 310°C.

For the case of CH-MS sample, the loss of water adsorbed on the zeolite (humidity) occurred at 109.98°C. It is convenient to highlight that there was no other peak corresponding to the loss of structural water for this sample, which occurred during the zeolite calcination at 500°C. It should be noted that other studies have reported the decomposition of NH_4Cl at 310°C [89]. Based on the DTG curve of CH-MS, it was concluded that this compound was not present in the modified zeolite. This finding could be due to the previous release of NH_3 in the calcination stage of the modification process, which was consistent with the FTIR results that confirmed the absence of this compound.

The chemical composition of CH-N and CH-MS is presented in Table 2. It can be observed that the weight

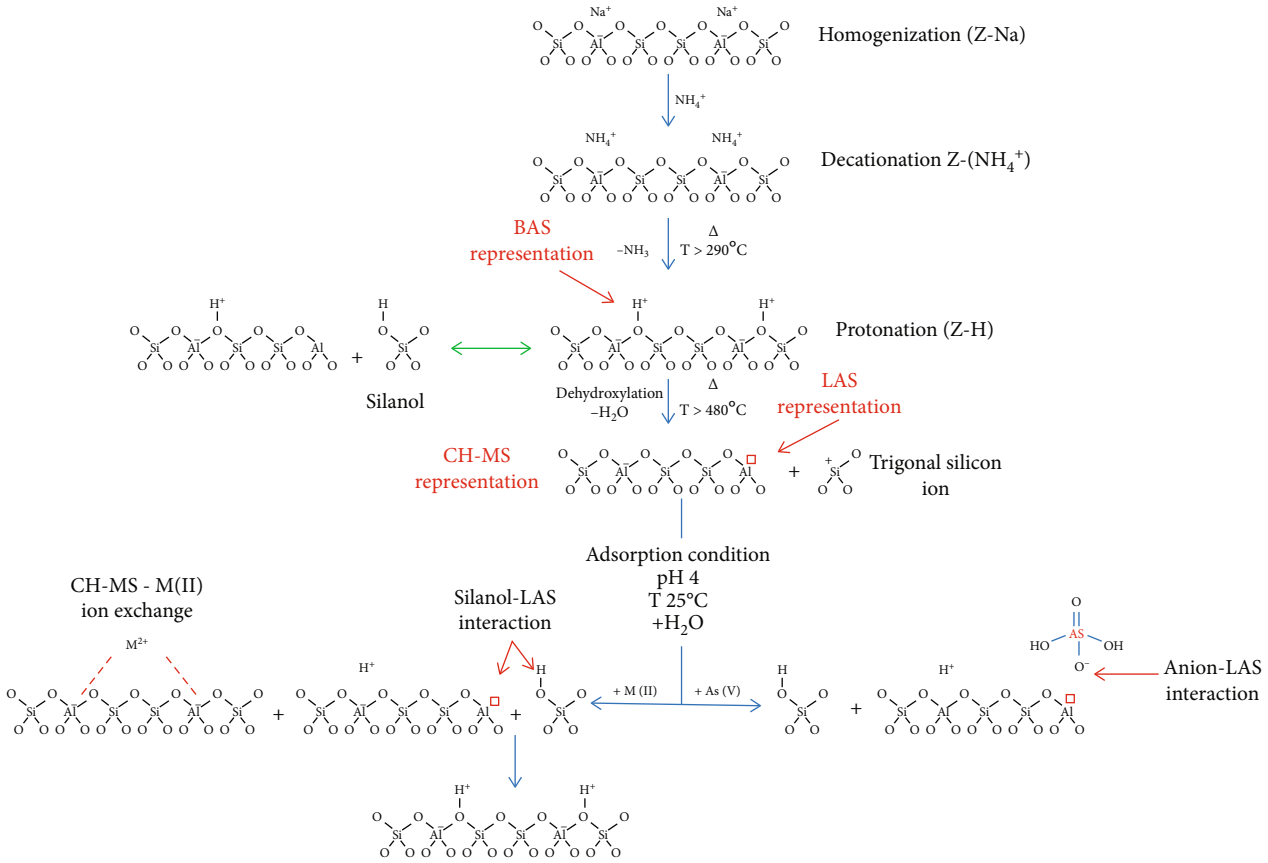

FIGURE 5: Illustrative 1D scheme of the stages of CH-N modification process where the formation of silanol, Brönsted acid sites (BAS), Lewis acid sites (LAS), and trigonal silicon ions is shown. The interaction of the CH-MS with divalent cations M(II) and anions like As(V). This figure was adapted from Uytterhoeven et al. [81] and Juzsakova et al. [45].

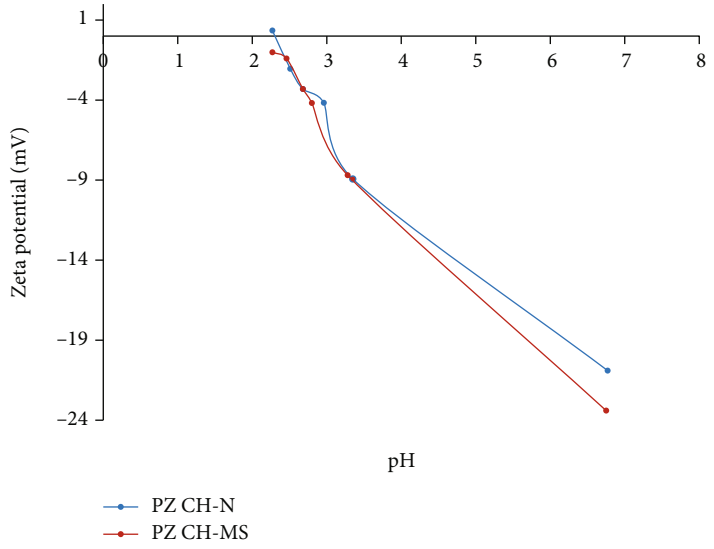

FIGURE 6: Zeta potential versus pH for CH-N and CH-MS samples.

fractions of exchangeable cations in CH-N decreased in the following order: Ca^{2+}, Mg^{2+}, Na^+, and K^+. On the other hand, the chemical composition confirmed the EDX results of CH-MS (Figure 2(d)) where the exchangeable cations Na^+ and Ca^+ were expelled out from the framework.

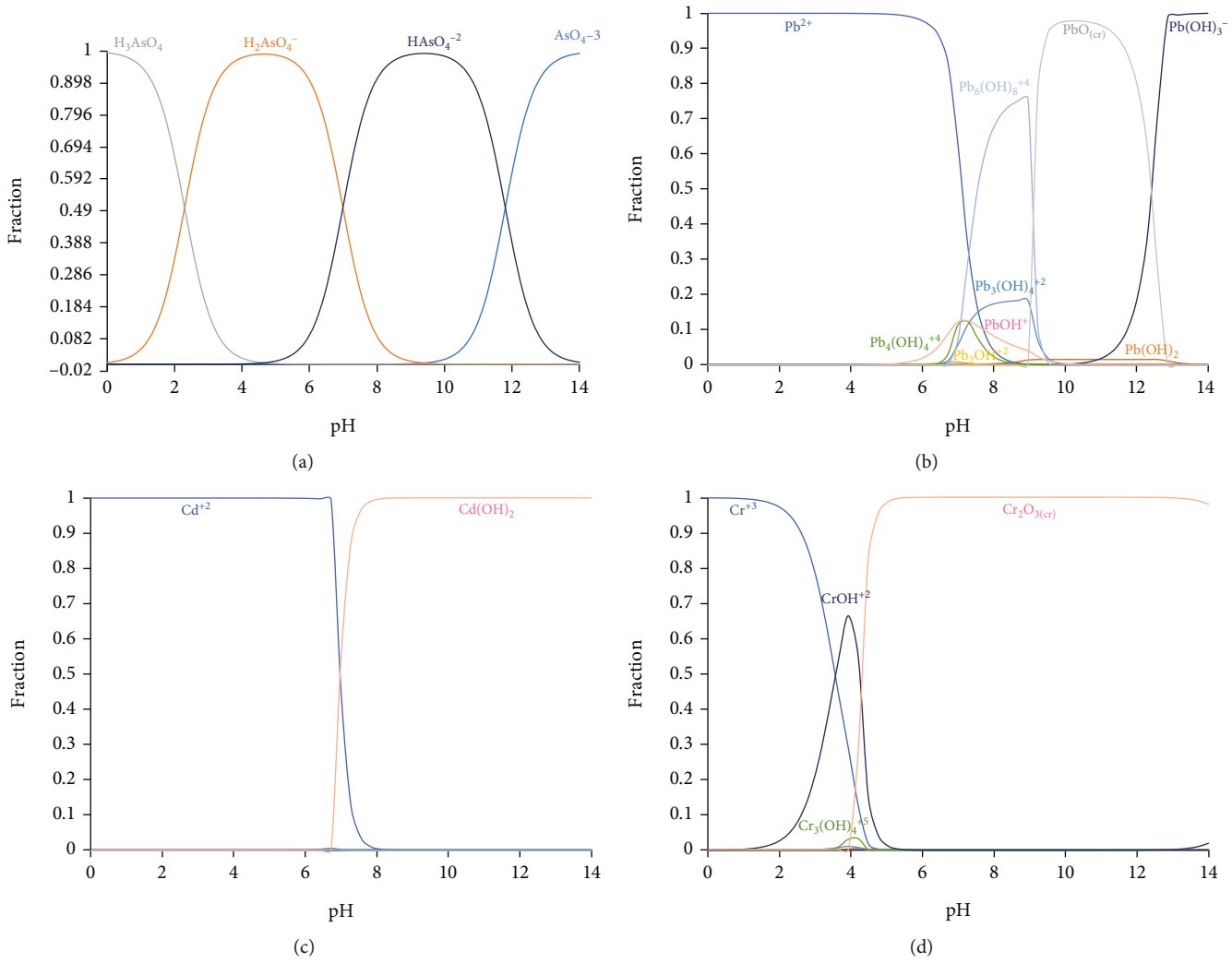

Figure 7: (a) Arsenic, (b) lead, (c) cadmium, and (d) chromium speciation as a function of solution pH in aqueous solution.

Table 2 shows Si/Al ratio of 3.3 for the CH-N sample that matched with the value of 3.2 found by Leyva-Ramos et al. [31], which was also between the range of 1.43-4.18, 3.2-3.8, and 2-4 obtained by Gottardi & Galli [90], Zamzow et al. [91], and Metwally & Attallah [92], respectively. Si/Al ratio of CH-MS sample was 2.8, which was lower than the value found for CH-N sample. The decrease in the Si/Al ratio of these samples coincided with the results reported by Panayotova [93] where a natural zeolite from Kardjali was modified by heating at 373°C and using 2 mol/dm^3 of NaOH solution.

The significant decrease in the Si/Al ratio between CH-N and CH-MS samples was caused by the superficial modification of the zeolite, whose steps are schematized in Figure 5. After homogenization (Z-Na) and decationization (Z-NH_4^+), NH_3 was removed by a thermal treatment at ≥290°C. This sample was named protonated form of zeolite (H-Z). This process generated BAS and was accompanied by the formation of free protons that attacked the tetrahedral aluminum lattice, thus causing the formal bond between aluminum and oxygen broken, and the corresponding formation of hydroxyl groups as silanol (Si-OH). This process was reversible since the interaction of silanols with aluminum formed the protonated zeolite and *vice versa* [79, 94]. Note that Iler [95] established that the condensation of silanol groups was higher in the presence of excess salts at pH 4-8. Therefore, the pH 7 and the application of 2 M NH_4Cl solution in the chabazite modification process provided the optimal conditions for the formation of silanol groups. They can be eliminated with the consecutive washing of material during the modification process. Therefore, it was reflected as an increase in the proportion of Al in the zeolite framework and a change in the Si/Al ratio.

3.2. Surface Properties of Zeolites. Figure 6 shows the results of the pH of PZ for both zeolites. It was concluded that the CH-N and CH-MS surfaces were negatively charged at tested adsorption conditions. Similar findings have been reported in the literature for clinoptilolite and other zeolites treated with NH_4Cl and calcination process [86, 96].

The negative charge for CH-MS was an expected result, which can be explained considering that the modification process was carried out at high temperature (i.e., 500°C).

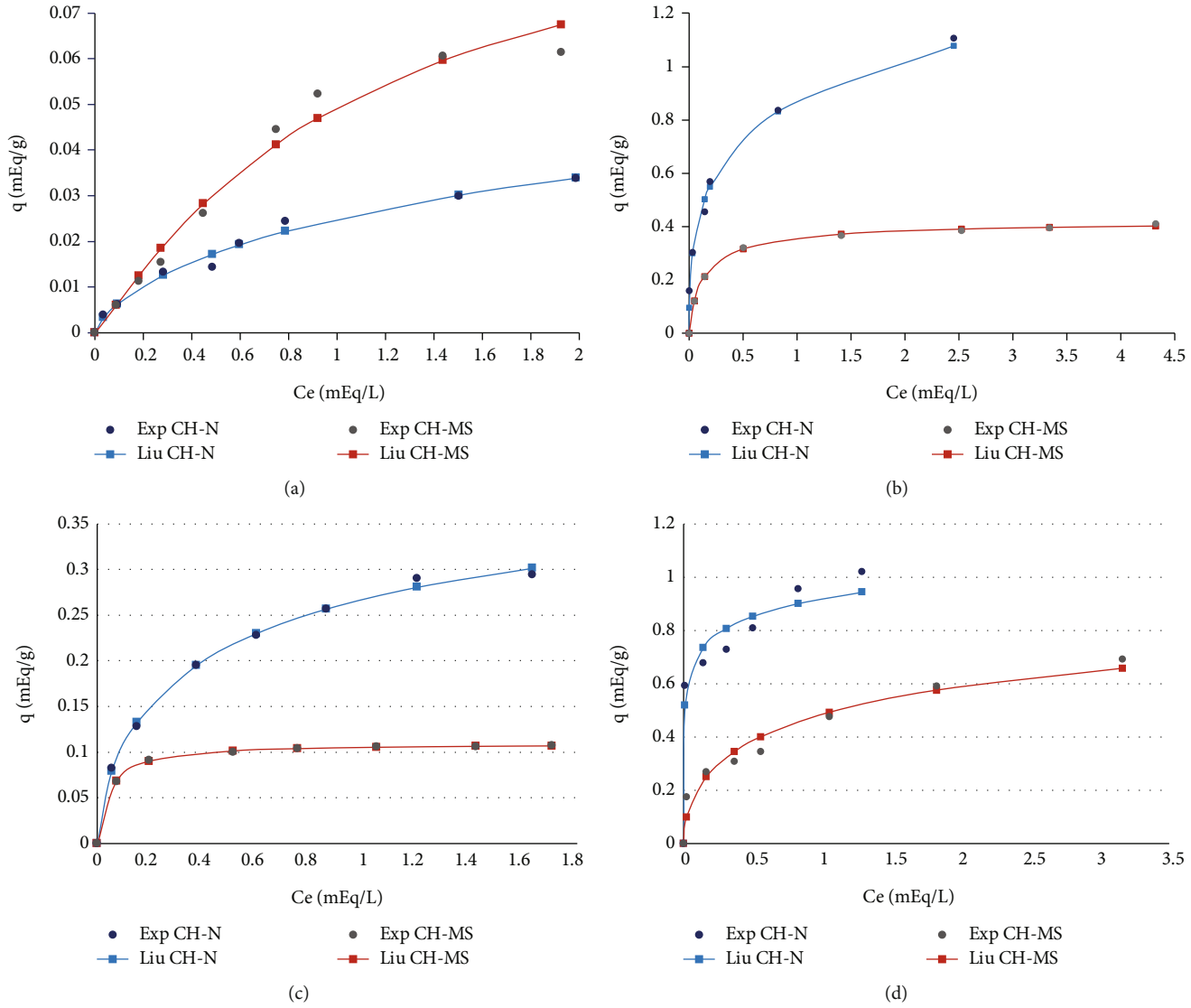

Figure 8: Isotherms for the adsorption of (a) As(V), (b) Pb(II), (c) Cd(II), and (d) Cr(III) on CH-N and CH-MS zeolites at pH 4 and their correlation with Liu model.

Ward [86] indicated that if the calcination process occurred at ≥480°C, BAS became LAS because the bounds of H-Z were very weak and easily removable (i.e., this process is called dehydroxylation or water loss). This phenomenon caused the formation of trigonal silicon ions and accessible trigonal aluminum [81] that can accept a pair of electrons, and therefore, it can adsorb anions. Figure 5 illustrates the formation of LAS where the negative charge of CH-MS is clearly outlined.

The surface interactions involved in the adsorption of anions on this modified zeolite can be explained as follows: CH-MS zeolite showed a negatively surface charge in the aqueous solutions that caused the attraction of H^+ ions from the solution, while the HO^- ions were attracted by the trigonal silicon ions, thus forming silanols. The adsorbate anions in the solution can interact via electrostatic attraction with the LAS [97] since they are the active sites in the zeolites [98]. This mechanism agreed with that proposed by Uytterhoeven [81] for water, Lewis acid centers, and molecules with lone pairs of electrons such as NH_3. On the other hand, the cations can be attracted by the negative charges of the CH-MS during the adsorption process. Note that the divalent cations could interact with more than a single site of the zeolite during the interface phenomenon [99]. It could be expected that the adsorption of cations on CH-MS was associated to an ion exchange. As explained, the interaction of silanol groups with acid centers of a zeolite generates a protonated zeolite. But this process was not reversible at 25°C because the zeolite was not reheated and the dehydroxylation did not occur.

CEC of CH-N and CH-MS was 1.68 and 0.53 mEq/g. These values showed a significant decrease of 68.45% of this property with respect to a CH-N sample. This result was because the ion exchange behavior of zeolites depends on the internal properties like chemical composition, framework

Table 3: Results of isotherm fitting using the Langmuir, Freundlich, Sips, and Liu equations for the adsorption of As(V), Pb(II), Cd(II), and Cr(III) on CH-N and CH-MS zeolites.

Ion	Zeolite	Model parameters*				R^2	%D	X^2	Model
		q_{model} (mg/g)	q_{model} (mEq/g)	K_{model}	n_{model}				
As(V)	CH-N			0.024	1.954	0.984	8.473	1.01×10^{-3}	Freundlich
		1.324	0.047	1.219		0.979	14.509	3.32×10^{-3}	Langmuir
		2.226	0.079	0.330	0.701	0.973	6.539	8.43×10^{-4}	Liu
		2.226	0.079	0.460	0.685	0.982	6.166	8.15×10^{-4}	Sips
As(V)	CH-MS			0.045	1.600	0.934	24.330	8.01×10^{-3}	Freundlich
		3.015	0.107	0.825		0.973	14.473	3.44×10^{-3}	Langmuir
		2.902	0.103	0.924	1.105	0.988	8.683	2.22×10^{-4}	Liu
		2.902	0.103	0.933	1.162	0.974	7.82	2.20×10^{-4}	Sips
Pb(II)	CH-N			0.851	3.008	0.992	11.949	0.056	Freundlich
		114.989	1.109	5.537		0.956	27.56	2.591	Langmuir
		235.960	2.277	0.307	0.0407	0.992	9.656	0.048	Liu
		232.429	2.244	0.635	0.410	0.989	9.778	0.049	Sips
Pb(II)	CH-MS			0.314	4.885	0.962	10.525	0.026	Freundlich
		42.279	0.408	7.576		0.995	2.219	1.27×10^{-3}	Langmuir
		43.656	0.421	5.365	0.864	0.997	1.136	4.36×10^{-4}	Liu
		43.656	0.421	6.976	0.864	0.998	1.135	4.36×10^{-4}	Sips
Cd(II)	CH-N			0.273	2.582	0.997	4.194	4.98×10^{-3}	Freundlich
		18.716	0.333	4.250		0.983	5.967	8.38×10^{-3}	Langmuir
		25.236	0.449	1.796	0.660	0.997	2.048	7.95×10^{-4}	Liu
		25.236	0.449	1.472	0.6604	0.995	2.047	7.95×10^{-4}	Sips
Cd(II)	CH-MS			0.104	8.139	0.882	4.564	1.63×10^{-3}	Freundlich
		6.126	0.109	23.016		0.995	0.716	5.29×10^{-5}	Langmuir
		6.126	0.109	22.54	1.051	0.996	0.632	4.76×10^{-5}	Liu
		6.126	0.109	26.10	1.047	0.996	0.631	4.77×10^{-5}	Sips
Cr(III)	CH-N			0.876	9.718	0.838	7.111	0.035	Freundlich
		19.680	0.855	190.38		0.441	12.302	0.090	Langmuir
		45.773	1.990	0.451	0.194	0.962	8.401	0.034	Liu
		44.719	1.944	0.889	0.195	0.809	8.397	0.035	Sips
Cr(III)	CH-MS			0.455	2.457	0.986	11.058	0.078	Freundlich
		17.259	0.750	2.049		0.914	20.917	0.671	Langmuir
		25.495	1.108	0.629	0.544	0.966	12.965	0.075	Liu
		24.434	1.062	0.842	0.559	0.941	13.310	0.0811	Sips

*q_{model} (q_L, q_{LF}, and q_S) is the maximum adsorption capacities of the Langmuir, Liu, and Sips equations. K_{model} (K_L, K_{LF}, K_S, and K_F) is the constant of the Langmuir, Liu, Sips (L/mEq), and Freundlich (mEq/g) $(L/mEq)^{1/nF}$ equations. n_{model} (n_{LF}, n_S, and n_F) is the dimensionless exponent of the Liu, Sips, and Freundlich equations.

structure, and charge density [100], besides the external properties like size, shape, charge, and concentration of ions [101]. As stablished by Jacobs and Leuven [102], the average reaction rate per site will be related with the chemical composition, thus generating an increment almost linearly of the frequency of silanol groups with a decrement of Si/Al ratio of the framework [103], which was coupled with the formation of LAS containing trigonal silicon ions. This explained that the change in the Si/Al ratio of CH-MS sample caused a decrement of the number of active sites because of the formation of the silanol groups and the trigonal silicon ions. This pointed out that the silanol groups were not active centers such these cannot serve as adsorption sites [80]. Although LAS were active sites, they can attract

Table 4: Maximum adsorption capacities for the removal of As(V), Pb(II), Cd(II), and Cr(III) using different materials.

Ion	Adsorbent	q_{max} (mg/g)	Isotherm model	Reference
As(V)	Clinoptilolite and modernite natural and modified with Fe	9.2×10^{-3} 0.062	Freundlich	Baskan & Pala [126] Velazquez-Peña et al. [128] Elizalde-González et al. [127]
	Chabazite modified with Fe and Zr	0.068	Freundlich	Velazquez-Peña et al. [128]
	Hydrated cement	1.92	Langmuir	Bibi et al. [129]
	Bone char	2.45	Langmuir	Alkurdi et al. [118]
	Activated carbon from oat hulls	3.09	Langmuir	Chuang et al. [134]
	Graphene oxide modified by iron-manganese binary oxide (FeMnOx/RGO)	11.5	Langmuir	Zhu et al. [135]
	Magnetite nanoparticle coated zeolite	19.39	Freundlich	Liu et al. [130]
	Carbon nanotubes coated with zirconium oxide	124.6		Liu et al. [131]
Pb(II)	Clinoptilolite	14.25-22.60	Freundlich	Kragović et al. [136] Mozgawa & Bajda [137]
	Cocoa pod husk and watermelon rind	20.10-98.06	Rendlich-Peterson	Liu et al. [138]
	Clinoptilolite natural and its $NH_4^+$and Na^+ forms	120.2-142.8	Langmuir	Leyva-Ramos et al. [139]
	Chabazite	175	—	Kesraoui-Ouki et al. [26]
	Synthetized zeolite from lithium leach residue via hydrothermal method	487.80	Langmuir	Lv et al. [140]
	Carbon foam	491.0	Sips	Lee et al. [141]
	Synthetized zeolite from bagasse fly ash	625.0	Langmuir	Jangkorn et al. [142]
Cd(II)	Erionite and clinoptilolite	2.54–4.63	Sips	Hernández-Montoya et al. [120]
	Peanut husk and corn stalk industrial waste	7.68-12.63	Langmuir	Rozumová et al. [143] Zheng et al. [107]
	Carbon nanotubes oxidized with HNO_3	11.1	—	Li et al. [144]
	Chabazite	13.26	Freundlich	Panuccio et al. [145]
	Synthesized coal fly ash zeolite	26.25	Langmuir	Javadian et al. [146]
	Fly ash treated with NaOH	48.31	Langmuir	Buema et al. [147]
	Activated carbon derived from bagasse	49.07	Freundlich	Mohan & Singh [148]
	Grape pomace activated carbon	75.61	Langmuir	Sardella et al. [149]
Cr(III)	Fibrous activated carbons	3.52	Langmuir	Aggarwal et al. [150]
	Granulated activated carbon	13.31	Langmuir	Aggarwal et al. [150]
	MnO_2-modified magnetic biochar derived from palm kernel cake	19.92	Langmuir	Maneechakr & Mongkollertlop [151]
	Natural clinoptilolite	21.20	—	Mozgawa & Bajda [137]
Cr(VI)	Multiwalled carbon nanotube	13.2	—	Kumar et al. [152]
	Magnetic zeolite/chitosan composites	25.67	Langmuir	Liu et al. [153]
	Porous Fe_3O_4 hollow microspheres/graphene oxide composite	32.33	Langmuir	Liu et al. [154]
	Functionalized multiwalled carbon nanotube with H_2SO_4/HNO_3 solution	85.83	—	Kumar et al. [152]
	Ionic liquid impregnated exfoliated graphene oxide	285.71	Temkin	Kumar et al. [155]

anions. As a result of the interaction of BAS and LAS, the zeolites present a superacidity [104] since both sites act synergistically potentiating the acidity [105]. As stablished by Barthomeuf [106], an acidic environment in zeolites affects the number of interchange sites, their location, density, and efficiency.

The value of CEC of CH-N was within the range of values reported for natural chabazites from Japan, Christmas Arizona, and a zeolite provided by American Colloid Co., which showed values of 1.87, 1.95, and between 0.08 and 2.61 mEq/g, respectively [20, 70, 107]. The decrease in CEC agreed with Ferrer [108] that used a clinoptilolite submitted to the same surface treatment and subsequent calcination at 500°C. These authors reported CEC values of 11.76 and 6.33 mEq/g for natural and modified materials, respectively. This treatment generated a change of 46% in this property,

which was lower than that obtained with chabazite. In this direction, Moreno-Tost et al. [109] use Cu-exchanged mordenite and clinoptilolite with the subsequent calcination at 550°C. These authors found a change in the CEC of 86% with respect to a natural clinoptilolite and 68% for natural modernite.

3.3. Analysis and Modeling of Adsorption Isotherms. Figure 7 shows the speciation diagrams of the different metals in the aqueous solution as a function of solution pH. The predominant ionic forms for tested adsorbates at pH 4 were Pb^{2+} and Cd^{2+} for Pb(II) and Cd(II), while $H_2AsO_4^-$ and $(CrOH)^{2+}$ were the dissolved species for As(V) and Cr(III) during the adsorption experiments. Therefore, the experimental isotherms of the adsorption of As(V), Pb(II), Cd(II), and Cr(III) on CH-N and CH-MS samples are reported in Figure 8, and the fitting results using the models of Langmuir, Freundlich, Sips, and Liu are shown in Table 3.

The adsorption capacity on CH-N and CH-MS followed the next sequence: Pb(II) > Cr(III) > Cd(II) > As(V), which agreed with the results obtained by Caputo and Pepe [32]. Experimental data showed that As(V) adsorption capacity was 0.034 and 0.061 mEq/g for CH-N and CH-MS, respectively, thus indicating that the zeolite functionalization improved in 79% its removal performance for this ion. Pb(II) adsorption capacities of CH-N and CH-MS were 1.10 and 0.41 mEq/g, respectively, while the Cd(II) and Cr(III) adsorption capacities of these zeolites were 0.29 and 0.11 mEq/g and 1.02 and 0.69 mEq/g, respectively. These reductions (33–67%) in the adsorption capacities of these cations were directly related to CEC decreased 68.45% due to the zeolite modification and the generation of BAS and LAS on the adsorbent surface. These adsorption capacities were not attributed to the surface area and pore diameter of tested zeolites, since both samples showed similar textural parameters.

The maximum exchange degree of Pb(II) on CH-N was an expected result, which can be explained according to the Eisenman-Sherry theory [110, 111]. Particularly, Pb(II) ion has a lower value of hydration enthalpy and a higher value of equilibrium constant (which is generally utilized as a measure of the cation exchange selectivity) in chabazite than those reported for the other two cations.

The chabazite has four classes of cation sites, named C1, C2, C3, and C4, where C1 sites are located in the center of the small cage (D6R) and they can be accessed through 6-membered ring, thus representing 20% of the overall CEC of this zeolite. C2-C4 sites are located in the large ellipsoidal cavities, and they can be accessed via 8-membered ring [112, 113]. According to the Double Selectivity Model (DSM) proposed by Pepe et al. [114], these types of sites are named group "I" and group "II." It could be expected that large ions like $(CrOH)^{2+}$ could not access to C1, while Pb(II) and Cd(II) can interact with these sites [115, 116]. So, the reduction of CEC in the modified zeolite was mainly associated to the loss of active sites in group I and group II, which were involved in the generation of Lewis acid centers. This phenomenon affected the final adsorption properties of the modified zeolite for cationic species. It is also important to mention that the significant reduction (up to 67%) of Pb(II) adsorption properties of CH-MS was associated to Na^+ ions that were expelled out from the zeolite framework during the modification process. Previous studies have reported that Na^+ can be completely exchangeable by Pb^{2+}, thus explaining the adsorption capacities of natural chabazite [116, 117].

Table 5: Calculated steric parameters for the adsorption of Cd(II), Pb(II), Cr(III), and As(V) on CH-N and CH-MS zeolites.

Adsorbate	Zeolite	n_{ads}	Interpretation
As(V)	CH-N	0.69	Multianchorage
	CH-MS	1.68	Multi-ionic
Pb(II)	CH-N	0.41	Multianchorage
	CH-MS	0.88	Multianchorage
Cd(II)	CH-N	0.68	Multianchorage
	CH-MS	0.89	Multianchorage
Cr(III)	CH-N	0.76	Multianchorage
	CH-MS	0.39	Multianchorage

Table 3 indicates that the q_L values obtained with the Langmuir model were lower than q_{LF} and q_S values calculated by the Liu and Sips models. These findings agreed with other studies reported for the adsorption of As(V), Pb(II), Cd(II), and Cr(III) ([118–121]). On the other hand, the n_F values of the Freundlich model ranged from 1.60 to 9.71 for the adsorption of tested ions, thus indicating a favorable removal process [54, 122]. The Langmuir constant K_L can be associated to the bonding energy between the zeolite and ions [123], and this parameter ranged from 1.21 to 190.38 (L/mEq), thus suggesting a good adsorption affinity between the zeolite and tested ions.

In terms of modeling, X^2 has been widely used to analyze the error distributions of data sets and to identify the most suitable equation for the calculation of adsorption isotherms [58, 124, 125]. Therefore, X^2 was employed to characterize the performance of tested isotherm models for both zeolites. This statistical metric indicated that the three-parameter isotherm models (i.e., Liu and Sips) showed the better fit of experimental data, thus presenting X^2 values lower than those obtained for the two-parameter isotherm models of Langmuir and Freundlich. Herein, it is convenient to recall that the use of the Sips equation is usually restricted to the fact that its dimensionless heterogeneity factor n_S must be between 0 and 1 [55, 122]. Results reported in Table 3 indicated that the calculated n_S values for As(V), Pb(II), Cd(II), and Cr(III) adsorption on chabazite modified did not comply with this restriction. Therefore, the Liu isotherm ($X^2 = 4.76 \times 10^{-5} - 0.075$) was selected as the best model to correlate these experimental adsorption isotherms (see Figure 8).

For illustration, Table 4 shows a comparison of the maximum adsorption capacity for the removal of different ions using several adsorbents. Overall, the results confirmed that the protonated chabazite was more effective for the removal of As(V) than other zeolites reported in the literature like clinoptilolite, modernite, and chabazite [126–128], as well as other waste materials like hydrated cement and bone char [118, 129]. However, the adsorption capacities of CH-N and CH-

MS were lower than the values reported for advanced materials like graphene oxide and carbon nanotubes [130, 131].

This study confirmed that the functionalization of zeolites to remove anions is a promising approach to improve the performance of these materials in water treatment. For example, the clinoptilolite modified with NH_4Cl plus its subsequent thermal treatment at 500°C increased its fluoride adsorption capacity by 2.33-fold with respect to the natural zeolite [37]. Other study showed that a natural zeolite rock treated at 800°C increased its anion adsorption capacity with respect to the uncalcined zeolite [39]. Another example is the thermal treatment (at ≥500) of different mesoporous silica sieves like MCM-41, MCM-48, SBA-15, and Co/MCM-41 to improve the removal of sulfur from diesel [132, 133].

With respect to the performance of natural chabazite for the removal of cations, its Pb(II) adsorption properties are competitive and can outperform the results obtained using watermelon rind and other zeolites like natural and modified clinoptilolite and chabazite [26, 138, 139]. Even after its functionalization, the protonated chabazite showed a Pb(II) adsorption capacity higher than those of cocoa pod husk and natural clinoptilolite [136–138]. However, this modified zeolite can be outperformed by, for example, carbon foam and zeolites synthesized by complex processes from lithium leach residue and bagasse fly ash ([135, 141, 142]).

For the case of Cd(II) adsorption, CH-MS can outperform erionite and clinoptilolite [120], while the adsorption properties of CH-N were better than those reported for carbon nanotubes and biomass wastes like peanut husk and corn stalk [143, 144, 156]. However, fly ash treated with NaOH outperformed this zeolite [147]. Also, the adsorption capacities of natural and modified chabazite for Cd(II) removal were significantly lower than those obtained with activated carbon [148, 149].

For the case of Cr(III) and Cr(VI) adsorption, CH-MS outperformed different activated carbons, magnetic zeolite/chitosan composites, multiwalled carbon nanotube, and natural clinoptilolite [137, 150–152]. On the other hand, the adsorption properties of CH-N were higher than those reported for magnetic zeolite/chitosan composites and porous Fe_3O_4 hollow microspheres/graphene oxide composite [153, 154]. However, its removal performance was lower than the reported for functionalized multiwalled carbon nanotube with H_2SO_4/HNO_3 solution and ionic liquid impregnated exfoliated graphene oxide [152, 155].

In summary, these results indicated that CH-MS could be considered a promising adsorbent for the removal of anions and cations from polluted water. This adsorbent could be applied in the depollution of other matrices like soil or mining waste, which also contain both types of ionic pollutants.

With respect to the interpretation of the adsorption mechanism, the steric parameters related to the adsorption of Cd(II), Pb(II), Cr(III), and As(V) on CH-N and CH-MS are reported in Table 5. In particular, n_{ads} ranged from 0.41 to 0.76 for the adsorption of cations and $n_{ads} = 0.69$ for the anion adsorption on CH-N. These results suggested that the removal of Cd(II), Pb(II), Cr(III), and As(V) can be classified as multianchorage where two adsorption sites from this zeolite could participate during the removal process [60]. For the case of modified chabazite, the calculated n_{ads} values ranged from 0.39 to 0.89 for the adsorption of heavy metal cations, while n_{ads} was 1.68 for the adsorption of As(V) anions (see Table 5). These results indicated that the Pb(II), Cd(II), and Cr(III) adsorption prevailed as multianchorage, and a multi-ionic adsorption occurred for the As(V) removal with CH-MS sample. The amount of adsorption sites of CH-N that were involved in the adsorption of these pollutants was 0.12-1.19 mEq/g, while the adsorption sites of CH-MS that participated in the adsorption were 0.04–0.48 mEq/g. These calculations were consistent with characterization results and CEC values that indicated the loss of some adsorption sites due to the zeolite modification protocol. As illustrated in Figure 5, the framework vacancy generated during the surface modification of chabazite allowed that its adsorption sites could interact with more than one As(V) anion, thus causing a multi-ionic adsorption of this pollutant.

4. Conclusions

This study has proved that a low-cost and straightforward protocol can be used to modify and tailor the surface properties of chabazite for the adsorption of anionic pollutants from aqueous solutions. This zeolite surface modification allowed to generate Lewis acid centers that could act as electron pair acceptors, thus increasing up to 79% the As(V) adsorption properties. However, the adsorption of Pb(II), Cd(II), and Cr(III) cations of this modified chabazite decreased 33-67%. This reduction of the cation adsorption properties was generated by a decrement of its cation exchange capacity and the loss of Na^+ exchange sites from zeolite surface. Statistical physics calculations indicated that the adsorption of all these ions on natural chabazite was a multianchorage phenomenon, while the As(V) adsorption on modified chabazite was a multi-ionic process. A reduction of the number of zeolite adsorption sites after surface functionalization was confirmed that affected the removal of cationic species. Natural chabazite can be considered an outstanding adsorbent for the Pb(II) removal with adsorption capacities higher than 100 mg/g. The application of this modified chabazite can be extended for the removal of other relevant anion pollutants from water. Further studies should be also focused on its application to depollute other real-life matrices (e.g., soil and wastewater) containing both anionic and cationic toxic compounds.

Data Availability

The data used to support the findings of this study are included within the article.

Conflicts of Interest

The authors declare that they have no conflicts of interest.

Acknowledgments

This work was funded by the Consejo Nacional de Ciencia y Tecnología (National Council of Science and Technology),

CONACYT, Mexico, through Grant PN 2015-01-1616 (attention to national problems financed by CONACYT).

Supplementary Materials

The supplementary information describes through a flow diagram the steps of chabazite modification. *(Supplementary Materials)*

References

[1] J. G. Paithankar, S. Saini, S. Dwivedi, A. Sharma, and D. K. Chowdhuri, "Heavy metal associated health hazards: an interplay of oxidative stress and signal transduction," *Chemosphere*, vol. 262, article 128350, 2021.

[2] S. Tasharrofi, Z. Rouzitalab, D. M. Maklavany et al., "Adsorption of cadmium using modified zeolite-supported nanoscale zero-valent iron composites as a reactive material for PRBs," *Science of the Total Environment*, vol. 736, article 139570, 2020.

[3] S. Afroze and T. K. Sen, "A review on heavy metal ions and dye adsorption from water by agricultural solid waste adsorbents," *Water, Air, & Soil Pollution*, vol. 229, no. 7, pp. 1–50, 2018.

[4] E. Gutiérrez-Segura, M. Solache-Ríos, A. Colín-Cruz, and C. Fall, "Comparison of cadmium adsorption by inorganic adsorbents in column systems," *Water, Air, & Soil Pollution*, vol. 225, no. 6, pp. 1–13, 2014.

[5] International Agency for Research on Cancer, "Beryllium, cadmium, mercury, and exposures in the glass," in *Apresentado Em: IARC Working Group on the Evaluation of Carcinogenic Risks to Humans*, pp. 1–415, IARC monographs on the evaluation of carcinogenic risks to humans, Lyon, 1993.

[6] M. Chen, Z. Xie, Y. Yang, B. Gao, and J. Wang, "Effects of calcium on arsenate adsorption and arsenate/iron bioreduction of ferrihydrite in stimulated groundwater," *International Journal of Environmental Research and Public Health*, vol. 19, no. 6, p. 3465, 2022.

[7] J. Y. Chung, S. D. Yu, and Y. S. Hong, "Environmental source of arsenic exposure," *Journal of Preventive Medicine and Public Health*, vol. 47, no. 5, pp. 253–257, 2014.

[8] G. Genchi, M. S. Sinicropi, G. Lauria, A. Carocci, and A. Catalano, "The effects of cadmium toxicity," *International Journal of Environmental Research and Public Health*, vol. 17, no. 11, p. 3782, 2020.

[9] N. Saint-Jacques, L. Parker, P. Brown, and T. J. Dummer, "Arsenic in drinking water and urinary tract cancers: a systematic review of 30 years of epidemiological evidence," *Environmental Health*, vol. 13, no. 1, pp. 1–32, 2014.

[10] M. Ulmanu, E. Marañón, Y. Fernández, L. Castrillón, I. Anger, and D. Dumitriu, "Removal of copper and cadmium ions from diluted aqueous solutions by low cost and waste material adsorbents," *Water, Air, and Soil Pollution*, vol. 142, no. 1, pp. 357–373, 2003.

[11] S. Wang and Y. Peng, "Natural zeolites as effective adsorbents in water and wastewater treatment," *Chemical Engineering Journal*, vol. 156, no. 1, pp. 11–24, 2010.

[12] S. E. Bailey, T. J. Olin, R. M. Bricka, and D. D. Adrian, "A review of potentially low-cost sorbents for heavy metals," *Water Research*, vol. 33, no. 11, pp. 2469–2479, 1999.

[13] M. Boehler, B. Zwickenpflug, J. Hollender, T. Ternes, A. Joss, and H. Siegrist, "Removal of micropollutants in municipal wastewater treatment plants by powder-activated carbon," *Water Science and Technology*, vol. 66, no. 10, pp. 2115–2121, 2012.

[14] R. Chikri, N. Elhadiri, M. Benchanaa, and Y. el maguana, "Efficiency of sawdust as low-cost adsorbent for dyes removal," *Journal of Chemistry*, vol. 2020, Article ID 8813420, 17 pages, 2020.

[15] R. T. Yang, *Adsorbents: Fundamentals and Applications*, John Wiley & Sons, 2003.

[16] L. F. de Magalhães, G. R. da Silva, and A. E. C. Peres, "Zeolite application in wastewater treatment," *Adsorption Science & Technology*, vol. 2022, article 4544104, pp. 1–26, 2022.

[17] P. Misaelides, "Application of natural zeolites in environmental remediation: a short review," *Microporous and Mesoporous Materials*, vol. 144, no. 1-3, pp. 15–18, 2011.

[18] M. Moshoeshoe, M. S. Nadiye-Tabbiruka, and V. Obuseng, "A review of the chemistry, structure, properties and applications of zeolites," *Am. J. Mater. Sci*, vol. 7, no. 5, pp. 196–221, 2017.

[19] E. Koudelková, Y. Ghrib, F. S. de Oliveira Ramos, P. Čičmanec, and R. Bulánek, "Adsorption and separation of the C3 hydrocarbons on cationic FER zeolites: effect of dual sites existence," *Microporous and Mesoporous Materials*, vol. 279, pp. 416–422, 2019.

[20] S. Kesraoui-Ouki, C. R. Cheeseman, and R. Perry, "Natural zeolite utilisation in pollution control: a review of applications to metals' effluents," *Journal of Chemical Technology & Biotechnology: International Research in Process, Environmental AND Clean Technology*, vol. 59, no. 2, pp. 121–126, 1994.

[21] M. W. Ackley, S. U. Rege, and H. Saxena, "Application of natural zeolites in the purification and separation of gases," *Microporous and Mesoporous Materials*, vol. 61, no. 1-3, pp. 25–42, 2003.

[22] M. Servatan, P. Zarrintaj, G. Mahmodi et al., "Zeolites in drug delivery: progress, challenges and opportunities," *Drug Discovery Today*, vol. 25, no. 4, pp. 642–656, 2020.

[23] J. Zhang, R. Singh, and P. A. Webley, "Alkali and alkaline-earth cation exchanged chabazite zeolites for adsorption based CO_2 capture," *Microporous and Mesoporous Materials*, vol. 111, no. 1-3, pp. 478–487, 2008.

[24] W. M. Meier, D. H. Olson, and C. Baerlocher, "Atlas of Zeolite Structure Types," *Zeolites*, vol. 17, no. (1-2), 1996.

[25] J. V. Smith, "Topochemistry of zeolites and related materials. 1. Topology and geometry," *Chemical Reviews*, vol. 88, no. 1, pp. 149–182, 1988.

[26] S. Kesraoui-Ouki, C. Cheeseman, and R. Perry, "Effects of conditioning and treatment of chabazite and clinoptilolite prior to lead and cadmium removal," *Environmental Science & Technology*, vol. 27, no. 6, pp. 1108–1116, 1993.

[27] S. M. Yakout and E. H. Borai, "Adsorption behavior of cadmium onto natural chabazite: batch and column investigations," *Desalination and Water Treatment*, vol. 52, no. 22-24, pp. 4212–4222, 2014.

[28] S. K. Ouki and M. Kavannagh, "Performance of natural zeolites for the treatment of mixed metal-contaminated effluents," *Waste Management & Research*, vol. 15, no. 4, pp. 383–394, 1997.

[29] E. Erdem, N. Karapinar, and R. Donat, "The removal of heavy metal cations by natural zeolites," *Journal of Colloid and Interface Science*, vol. 280, no. 2, pp. 309–314, 2004.

[30] G. Galamini, G. Ferretti, V. Medoro, N. Tescaro, B. Faccini, and M. Coltorti, "Isotherms, kinetics, and thermodynamics of nh4+ adsorption in raw liquid manure by using natural chabazite zeolite-rich tuff," *Water*, vol. 12, no. 10, p. 2944, 2020.

[31] R. Leyva-Ramos, J. E. Monsivais-Rocha, A. Aragon-Piña et al., "Removal of ammonium from aqueous solution by ion exchange on natural and modified chabazite," *Journal of Environmental Management*, vol. 91, no. 12, pp. 2662–2668, 2010.

[32] D. Caputo and F. Pepe, "Experiments and data processing of ion exchange equilibria involving Italian natural zeolites: a review," *Microporous and Mesoporous Materials*, vol. 105, no. 3, pp. 222–231, 2007.

[33] X. Song, Y. Zhang, X. Cui, F. Liu, and H. Zhao, "Preparation and characterization of chabazite from construction waste and application as an adsorbent for methylene blue," *Adsorption Science & Technology*, vol. 2021, article 9994079, pp. 1–13, 2021.

[34] J. Wang, H. Zhao, G. Haller, and Y. Li, "Recent advances in the selective catalytic reduction of NOx with NH_3 on Cu-Chabazite catalysts," *Applied Catalysis B: Environmental*, vol. 202, pp. 346–354, 2017.

[35] M. I. Gallegos-García, *Modificación química de una zeolita tipo chabasita para la remoción de aniones en solución acuosa, [Doctoral thesis]*, UASLP, 2016.

[36] K. Barczyk, W. Mozgawa, and M. Król, "Studies of anions sorption on natural zeolites," *Spectrochimica Acta Part A: Molecular and Biomolecular Spectroscopy*, vol. 133, pp. 876–882, 2014.

[37] B. G. Saucedo-Delgado, D. A. De Haro-Del Rio, L. M. González-Rodríguez et al., "Fluoride adsorption from aqueous solution using a protonated clinoptilolite and its modeling with artificial neural network-based equations," *Journal of Fluorine Chemistry*, vol. 204, pp. 98–106, 2017.

[38] L. Zhu, X. Lv, S. Tong et al., "Modification of zeolite by metal and adsorption desulfurization of organic sulfide in natural gas," *Journal of Natural Gas Science and Engineering*, vol. 69, article 102941, 2019.

[39] A. T. Ahmed and H. Almohamadi, "Chemical and microstructural studies for using natural zeolite in advanced wastewater treatment," *International journal of Environmental Science and Technology*, pp. 1–8, 2022.

[40] V. J. Fernandes, A. S. Araujo, R. A. Medeiros et al., "Kinetic parameters of polyethylene degradation by the natural zeolite chabazite," *Journal of Thermal Analysis and Calorimetry*, vol. 56, no. 3, pp. 1279–1282, 1999.

[41] G. Piccini, M. Alessio, J. Sauer et al., "Accurate adsorption thermodynamics of small alkanes in zeolites. Ab initio theory and experiment for H-chabazite," *The Journal of Physical Chemistry C*, vol. 119, no. 11, pp. 6128–6137, 2015.

[42] B. R. Florindo, G. L. Catuzo, and L. Martins, "Porosity of CHA zeolite driving the formation of polyaromatic coke species in the methanol to olefins reaction," *Journal of the Brazilian Chemical Society*, vol. 32, pp. 1051–1059, 2021.

[43] N. Ghasemian, C. Falamaki, and M. Kalbasi, "Clinoptilolite zeolite as a potential catalyst for propane-SCR-NOx: performance investigation and kinetic analysis," *Chemical Engineering Journal*, vol. 236, pp. 464–470, 2014.

[44] C. D. R. Oliveira and J. Rubio, "Adsorption of ions onto treated natural zeolite," *Materials Research*, vol. 10, no. 4, pp. 407–412, 2007.

[45] T. Juzsakova, A. Csavdari, Á. Rédey et al., "Study on the alkylaton mechanism of isobutane with 1-butene using environmental friendly catalysts," *Environmental Engineering and Management Journal*, vol. 13, no. 9, pp. 2343–2347, 2014.

[46] D. R. Corbin, B. F. Burgess, A. J. Vega, and R. D. Farlee, "Comparison of analytical techniques for the determination of silicon and aluminum content in zeolites," *Analytical Chemistry*, vol. 59, no. 22, pp. 2722–2728, 1987.

[47] D. W. Ming and J. B. Dixon, "Quantitative determination of clinoptilolite in soils by a cation-exchange capacity method," *Clays and Clay Minerals*, vol. 35, no. 6, pp. 463–468, 1987.

[48] L. A. Bernal-Jácome, L. Olvera-Izaguirre, M. Gallegos García, R. Delgado-Delgado, and M. Á. Espinosa Rodríguez, "Adsorption of lead (II) from aqueous solution using adsorbents obtained from nanche stone (Byrsonima crassifolia)," *Journal of the Mexican Chemical Society*, vol. 64, no. 4, pp. 301–315, 2020.

[49] D. Nityanandi and C. V. Subbhuraam, "Adsorptive removal of Pb (II) ions from aqueous solution using a coir-based product (puresorbe)," *Adsorption Science & Technology*, vol. 24, no. 2, pp. 177–192, 2006.

[50] U. Wingenfelder, C. Hansen, G. Furrer, and R. Schulin, "Removal of heavy metals from mine waters by natural zeolites," *Environmental Science & Technology*, vol. 39, no. 12, pp. 4606–4613, 2005.

[51] A. Bedemo, B. S. Chandravanshi, and F. Zewge, "Removal of trivalent chromium from aqueous solution using aluminum oxide hydroxide," *Springerplus*, vol. 5, no. 1, pp. 1–11, 2016.

[52] M. H. Ehrampoush, M. Miria, M. H. Salmani, and A. H. Mahvi, "Cadmium removal from aqueous solution by green synthesis iron oxide nanoparticles with tangerine peel extract," *Journal of Environmental Health Science and Engineering*, vol. 13, no. 1, pp. 1–7, 2015.

[53] I. Langmuir, "The adsorption of gases on plane surfaces of glass, mica and platinum," *Journal of the American Chemical Society*, vol. 40, no. 9, pp. 1361–1403, 1918.

[54] H. M. F. Freundlich, "Over the adsorption in solution," *The Journal of Physical Chemistry*, vol. 57, no. 385471, pp. 1100–1107, 1906.

[55] R. Sips, "On the structure of a catalyst surface," *The Journal of Chemical Physics*, vol. 16, no. 5, pp. 490–495, 1948.

[56] Y. Liu, H. Xu, S. F. Yang, and J. H. Tay, "A general model for biosorption of Cd^{2+}, Cu^{2+} and Zn^{2+} by aerobic granules," *Journal of Biotechnology*, vol. 102, no. 3, pp. 233–239, 2003.

[57] M. Rahman, A. Pal, K. Uddin, K. Thu, and B. B. Saha, "*Statistical analysis of optimized isotherm model for maxsorb iii/ethanol and silica gel/water pairs*," *Evergreen*, vol. 5, no. 4, pp. 1–12, 2018.

[58] B. Boulinguiez, P. Le Cloirec, and D. Wolbert, "Revisiting the determination of Langmuir parameters. Application to Tetrahydrothiophene adsorption onto activated carbon," *Langmuir*, vol. 24, no. 13, pp. 6420–6424, 2008.

[59] R. Leyva-Ramos, A. Jacobo-Azuara, P. E. Diaz-Flores, R. M. Guerrero-Coronado, J. Mendoza-Barron, and M. S. Berber-Mendoza, "Adsorption of chromium(VI) from an aqueous solution on a surfactant-modified zeolite," *Colloids and Surfaces A: Physicochemical and Engineering Aspects*, vol. 330, no. 1, pp. 35–41, 2008.

[60] O. Amrhar, L. El Gana, and M. Mobarak, "Calculation of adsorption isotherms by statistical physics models: a review,"

Environmental Chemistry Letters, vol. 19, no. 6, pp. 4519–4547, 2021.

[61] D. K. Arkhipenko, G. P. Valueva, and T. N. Moroz, "Determination of the space group of chabazite," *Journal of Structural Chemistry*, vol. 36, no. 1, pp. 171–174, 1995.

[62] M. M. Treacy and J. B. Higgins, *Collection of simulated xrd powder patterns for zeolites fifth (5th)*, Elsevier, 5th edition, 2007.

[63] A. K. Bansiwal, S. S. Rayalu, N. K. Labhasetwar, A. A. Juwarkar, and S. Devotta, "Surfactant-modified zeolite as a slow release fertilizer for phosphorus," *Journal of Agricultural and Food Chemistry*, vol. 54, no. 13, pp. 4773–4779, 2006.

[64] A. Mohammadi, B. Bina, A. Ebrahimi, Y. Hajizadeh, M. M. Amin, and H. Pourzamani, "Effectiveness of nanozeolite modified by cationic surfactant in the removal of disinfection by-product precursors from water solution," *International journal of environmental health engineering*, vol. 1, no. 1, p. 3, 2012.

[65] M. Osacký, H. Pálková, P. Hudec, A. Czímerová, D. Galusková, and M. Vítková, "Effect of alkaline synthesis conditions on mineralogy, chemistry and surface properties of phillipsite, P and X zeolitic materials prepared from fine powdered perlite by-product," *Microporous and Mesoporous Materials*, vol. 294, article 109852, 2020.

[66] M. R. Abukhadra, M. G. Basyouny, A. M. El-Sherbeeny, and M. A. El-Meligy, "The effect of different green alkali modification processes on the clinoptilolite surface as adsorbent for ammonium ions; characterization and application," *Microporous and Mesoporous Materials*, vol. 300, article 110145, 2020.

[67] E. Alvarez-Ayuso, A. Garcıa-Sánchez, and X. Querol, "Purification of metal electroplating waste waters using zeolites," *Water Research*, vol. 37, no. 20, pp. 4855–4862, 2003.

[68] B. E. Alver and M. Sakızcı, "Hydrogen (H_2) adsorption on natural and cation-exchanged clinoptilolite, mordenite and chabazite," *International Journal of Hydrogen Energy*, vol. 44, no. 13, pp. 6748–6755, 2019.

[69] A. Al-Mamoori, M. Alsalbokh, S. Lawson, A. A. Rownaghi, and F. Rezaei, "Development of bismuth-mordenite adsorbents for iodine capture from off-gas streams," *Chemical Engineering Journal*, vol. 391, article 123583, 2020.

[70] A. S. Sheta, A. M. Falatah, M. S. Al-Sewailem, E. M. Khaled, and A. S. H. Sallam, "Sorption characteristics of zinc and iron by natural zeolite and bentonite," *Microporous and Mesoporous Materials*, vol. 61, no. 1-3, pp. 127–136, 2003.

[71] T. M. Albayati and K. R. Kalash, "Polycyclic aromatic hydrocarbons adsorption from wastewater using different types of prepared mesoporous materials MCM-41in batch and fixed bed column," *Process Safety and Environmental Protection*, vol. 133, pp. 124–136, 2020.

[72] N. Mori, S. Nishiyama, S. Tsuruya, and M. Masai, "Deactivation of zeolites in n-hexane cracking," *Applied Catalysis*, vol. 74, no. 1, pp. 37–52, 1991.

[73] N. A. Atiyah, T. M. Albayati, and M. A. Atiya, "Interaction behavior of curcumin encapsulated onto functionalized SBA-15 as an efficient carrier and release in drug delivery," *Journal of Molecular Structure*, vol. 1260, article 132879, 2022.

[74] C. Giampaolo, L. Mengarelli, E. Torracca, and C. Spencer, "Zeolite characterization of "Vico red tuff with black scoria" ignimbrite flow: the extractive district of Civita Castellana (Viterbo, Italy)," *Il Nuovo Cimento B*, vol. 123, pp. 1459–1476, 2008.

[75] K. M. Ibrahim, H. N. Khoury, and R. Tuffaha, "Mo and Ni removal from drinking water using zeolitic tuff from Jordan," *Minerals*, vol. 6, no. 4, p. 116, 2016.

[76] R. M. Barrer, J. A. Davies, and L. V. C. Rees, "Thermodynamics and thermochemistry of cation exchange in chabazite," *Journal of Inorganic and Nuclear Chemistry*, vol. 31, no. 1, pp. 219–232, 1969.

[77] Y. Akdeniz and S. Ülkü, "Thermal stability of Ag-exchanged clinoptilolite rich mineral," *Journal of Thermal Analysis and Calorimetry*, vol. 94, no. 3, pp. 703–710, 2008.

[78] H. Aysan, S. Edebali, C. Ozdemir, M. C. Karakaya, and N. Karakaya, "Use of chabazite, a naturally abundant zeolite, for the investigation of the adsorption kinetics and mechanism of methylene blue dye," *Microporous and Mesoporous Materials*, vol. 235, pp. 78–86, 2016.

[79] J. W. Ward, "The nature of active sites on zeolites: II. Temperature dependence of the infrared spectra of hydrogen Y zeolite," *Journal of Catalysis*, vol. 9, no. 4, pp. 396–402, 1967.

[80] E. A. Paukshtis, M. A. Yaranova, I. S. Batueva, and B. S. Bal'zhinimaev, "A FTIR study of silanol nests over mesoporous silicate materials," *Microporous and Mesoporous Materials*, vol. 288, article 109582, 2019.

[81] J. B. Uytterhoeven, L. G. Christner, and W. K. Hall, "Studies of the hydrogen held by solids. VIII. The decationated zeolites," *The Journal of Physical Chemistry*, vol. 69, no. 6, pp. 2117–2126, 1965.

[82] J. W. Ward, "The nature of active sites on zeolites: III. The alkali and alkaline earth ion-exchanged forms," *Journal of Catalysis*, vol. 10, no. 1, pp. 34–46, 1968.

[83] C. Jia, P. Massiani, and D. Barthomeuf, "Characterization by infrared and nuclear magnetic resonance spectroscopies of calcined beta zeolite," *Journal of the Chemical Society, Faraday Transactions*, vol. 89, no. 19, pp. 3659–3665, 1993.

[84] R. Silva-Rodrigo, T. López-Goerne, V. Bertin-Mardel, R. Gómez-Romero, and P. Salas-Castillo, "Propiedades ácidas de los catalizadores de Pt-Sn/Al_2O_3 preparados por sol-gel," *Revista Mexicana de Ingeniería Química*, vol. 4, no. 2, pp. 141–145, 2005.

[85] C. A. Emeis, "Determination of integrated molar extinction coefficients for infrared absorption bands of pyridine adsorbed on solid acid catalysts," *Journal of Catalysis*, vol. 141, no. 2, pp. 347–354, 1993.

[86] J. W. Ward, "The nature of active sites on zeolites: VIII. Rare earth Y zeolite," *Journal of Catalysis*, vol. 13, no. 3, pp. 321–327, 1969.

[87] W. Wu and E. Weitz, "Modification of acid sites in ZSM-5 by ion-exchange: an in-situ FTIR study," *Applied Surface Science*, vol. 316, pp. 405–415, 2014.

[88] J. L. Stakebake, "Characterization of natural chabazite and 5A synthetic zeolites: part I. Thermal and outgassing properties," *Journal of Colloid and Interface Science*, vol. 99, no. 1, pp. 41–49, 1984.

[89] H. G. Stewart, T. D. Humphries, D. A. Sheppard et al., "Ammonium chloride–metal hydride based reaction cycle for vehicular applications," *Journal of Materials Chemistry A*, vol. 7, no. 9, pp. 5031–5042, 2019.

[90] G. Gottardi and E. Galli, *Natural Zeolites*, Springer Science & Business Media, 2012.

[91] M. J. Zamzow, B. R. Eichbaum, K. R. Sandgren, and D. E. Shanks, "Removal of heavy metals and other cations from wastewater using zeolites," *Separation Science and Technology*, vol. 25, no. 13-15, pp. 1555–1569, 1990.

[92] S. S. Metwally and M. F. Attallah, "Impact of surface modification of chabazite on the sorption of iodine and molybdenum radioisotopes from liquid phase," *Journal of Molecular Liquids*, vol. 290, article 111237, 2019.

[93] M. I. Panayotova, "Use of zeolite for cadmium removal from wastewater," *Journal of Environmental Science & Health Part A*, vol. 35, no. 9, pp. 1591–1601, 2000.

[94] B. V. Liengme and W. K. Hall, "Studies of hydrogen held by solids. Part *11.—Interaction of simple olefins and pyridine with decationated zeolites*," *Transactions of the Faraday Society*, vol. 62, pp. 3229–3243, 1966.

[95] R. K. Iler, "The colloid chemistry of silica and silicates," *Soil Science*, vol. 80, no. 1, p. 86, 1955.

[96] A. Corma, "Catálisis con zeolitas: desde el laboratorio a su aplicación industrial," *Arbor*, vol. 187, no. Extra_1, pp. 83–102, 2011.

[97] H. L. Jamieson, H. Yin, A. Waller, A. Khosravi, and M. L. Lind, "Impact of acids on the structure and composition of Linde type A zeolites for use in reverse osmosis membranes for recovery of urine-containing wastewaters," *Microporous and Mesoporous Materials*, vol. 201, pp. 50–60, 2015.

[98] J. Turkevich, F. Nozaki, and D. N. Stamires, "Proc. 3rd Internat. Congress Catalys., Amsterdam, 1964. *North-Holland publishing co*," *Amsterdam*, vol. 1, pp. 586–599, 1965.

[99] F. N. Murrieta-Rico, J. Antúnez-García, R. I. Yocupicio-Gaxiola, D. H. Galván, J. C. González, and V. Petranovskii, "Zeolites as initial structures for the preparation of functional materials," *Journal Of Applied Research And Technology*, vol. 20, no. 1, pp. 92–116, 2022.

[100] F. Yi, D. Xu, Z. Tao et al., "Correlation of Brønsted acid sites and Al distribution in ZSM-5 zeolites and their effects on butenes conversion," *Fuel*, vol. 320, article 123729, 2022.

[101] D. Kalló, "Applications of natural zeolites in water and wastewater treatment," *Reviews in Mineralogy and Geochemistry*, vol. 45, no. 1, pp. 519–550, 2001.

[102] P. A. Jacobs and K. U. Leuven, "Acid zeolites: an attempt to develop unifying concepts (P. H. Emmett award address, 1981)," *Catalysis Reviews*, vol. 24, no. 3, pp. 415–440, 1982.

[103] P. A. Jacobs, W. J. Mortier, and J. B. Uytterhoeven, "Properties of zeolites in relation to their electronegativity: acidity, carboniogenic activity and strength of interaction in transition metal complexes," *Journal of Inorganic and Nuclear Chemistry*, vol. 40, no. 11, pp. 1919–1923, 1978.

[104] P. A. Jacobs, *Carboniogenic Activity of Zeolites*, Elsevier Scientific Publishing Company, Amsterdam/Oxford/New York, 1977.

[105] S. Li, A. Zheng, Y. Su et al., "Brønsted/Lewis acid synergy in dealuminated HY zeolite: a combined solid-state NMR and theoretical calculation study," *Journal of the American Chemical Society*, vol. 129, no. 36, pp. 11161–11171, 2007.

[106] D. Barthomeuf, "Zeolite acidity dependence on structure and chemical environment. Correlations with catalysis," *Materials Chemistry and Physics*, vol. 17, no. 1-2, pp. 49–71, 1987.

[107] Y. Zeng, H. Woo, G. Lee, and J. Park, "Removal of chromate from water using surfactant modified Pohang clinoptilolite and Haruna chabazite," *Desalination*, vol. 257, no. 1-3, pp. 102–109, 2010.

[108] R. Ferrer-Luna, *Estudio sobre la estabilización fisicoquímica de metales pesados en suelo contaminado por jales mineros usando zeolita Clinoptilolita, [Master's thesis]*, UANL, 2018.

[109] R. Moreno-Tost, J. Santamaría-González, E. Rodríguez-Castellón et al., "Selective catalytic reduction of nitric oxide by ammonia over cu-exchanged Cuban natural zeolites," *Applied Catalysis B: Environmental*, vol. 50, no. 4, pp. 279–288, 2004.

[110] G. Eisenman, "Cation selective glass electrodes and their mode of operation," *Biophysical Journal*, vol. 2, no. 2, pp. 259–323, 1962.

[111] H. S. Sherry, "The ion-exchange properties of zeolites. I. Univalent ion exchange in synthetic faujasite," *The Journal of Physical Chemistry*, vol. 70, no. 4, pp. 1158–1168, 1966.

[112] A. Alberti, E. Galli, G. Vezzalini, E. Passaglia, and P. F. Zanazzi, "Position of cations and water molecules in hydrated chabazite. Natural and Na-, Ca-, Sr- and K-exchanged chabazites," *Zeolites*, vol. 2, no. 4, pp. 303–309, 1982.

[113] M. Calligaris, G. Nardin, L. Randaccio, and P. C. Chiaramonti, "Cation-site location in a natural chabazite," *Acta Crystallographica Section B: Structural Crystallography and Crystal Chemistry*, vol. 38, no. 2, pp. 602–605, 1982.

[114] F. Pepe, D. Caputo, and C. Colella, "The double selectivity model for the description of ion-exchange equilibria in zeolites," *Industrial & Engineering Chemistry Research*, vol. 42, no. 5, pp. 1093–1097, 2003.

[115] M. Calligaris and G. Nardin, "Cation site location in hydrated chabazites. Crystal structure of barium- and cadmium-exchanged chabazites," *Zeolites*, vol. 2, no. 3, pp. 200–204, 1982.

[116] F. Lucolano, D. Caputo, F. Pepe, and C. Colella, "A thermodynamic model of chabazite selectivity for Pb^{2+}," in *Studies in Surface Science and Catalysis*, vol. 155, pp. 339–346, Elsevier, 2005.

[117] E. Torracca, P. Galli, M. Pansini, and C. Colella, "Cation exchange reactions of a sedimentary chabazite," *Microporous and Mesoporous Materials*, vol. 20, no. 1-3, pp. 119–127, 1998.

[118] S. S. Alkurdi, R. A. Al-Juboori, J. Bundschuh, L. Bowtell, and A. Marchuk, "Inorganic arsenic species removal from water using bone char: a detailed study on adsorption kinetic and isotherm models using error functions analysis," *Journal of Hazardous Materials*, vol. 405, article 124112, 2021.

[119] A. Günay, E. Arslankaya, and I. Tosun, "Lead removal from aqueous solution by natural and pretreated clinoptilolite: adsorption equilibrium and kinetics," *Journal of Hazardous Materials*, vol. 146, no. 1-2, pp. 362–371, 2007.

[120] V. Hernández-Montoya, M. A. Pérez-Cruz, D. I. Mendoza-Castillo, M. R. Moreno-Virgen, and A. Bonilla-Petriciolet, "Competitive adsorption of dyes and heavy metals on zeolitic structures," *Journal of Environmental Management*, vol. 116, pp. 213–221, 2013.

[121] T. Guimarães, L. D. Paquini, B. R. L. Ferraz, L. P. R. Profeti, and D. Profeti, "Efficient removal of Cu(II) and Cr(III) contaminants from aqueous solutions using marble waste powder," *Journal of Environmental Chemical Engineering*, vol. 8, no. 4, article 103972, 2020.

[122] É. C. Lima, M. H. Dehghani, A. Guleria et al., "Adsorption: fundamental aspects and applications of adsorption for

effluent treatment," *In Green Technologies for the Defluoridation of Water, Elsevier*, pp. 41–88, 2021.

[123] M. I. Panayotova, "Kinetics and thermodynamics of copper ions removal from wastewater by use of zeolite," *Waste Management*, vol. 21, no. 7, pp. 671–676, 2001.

[124] M. Arshadi, M. J. Amiri, and S. Mousavi, "Kinetic, equilibrium and thermodynamic investigations of Ni(II), Cd(II), Cu(II) and Co(II) adsorption on barley straw ash," *Water Resources And Industry*, vol. 6, pp. 1–17, 2014.

[125] Y. He, L. Zhang, X. An, G. Wan, W. Zhu, and Y. Luo, "Enhanced fluoride removal from water by rare earth (La and Ce) modified alumina: adsorption isotherms, kinetics, thermodynamics and mechanism," *Science of the Total Environment*, vol. 688, pp. 184–198, 2019.

[126] M. B. Baskan and A. Pala, "Removal of arsenic from drinking water using modified natural zeolite," *Desalination*, vol. 281, pp. 396–403, 2011.

[127] M. P. Elizalde-González, J. Mattusch, W. D. Einicke, and R. Wennrich, "Sorption on natural solids for arsenic removal," *Chemical Engineering Journal*, vol. 81, no. 1-3, pp. 187–195, 2001.

[128] G. C. Velazquez-Peña, M. Solache-Ríos, M. T. Olguin, and C. Fall, "As(V) sorption by different natural zeolite frameworks modified with Fe, Zr and FeZr," *Microporous and Mesoporous Materials*, vol. 273, pp. 133–141, 2019.

[129] S. Bibi, A. Farooqi, K. Hussain, and N. Haider, "Evaluation of industrial based adsorbents for simultaneous removal of arsenic and fluoride from drinking water," *Journal of Cleaner Production*, vol. 87, pp. 882–896, 2015.

[130] C. H. Liu, Y. H. Chuang, T. Y. Chen et al., "Mechanism of arsenic adsorption on magnetite nanoparticles from water: thermodynamic and spectroscopic studies," *Environmental Science & Technology*, vol. 49, no. 13, pp. 7726–7734, 2015.

[131] D. Liu, S. Deng, A. Maimaiti et al., "As(III) and As(V) adsorption on nanocomposite of hydrated zirconium oxide coated carbon nanotubes," *Journal of Colloid and Interface Science*, vol. 511, pp. 277–284, 2018.

[132] A. T. Khadim, T. M. Albayati, and N. M. C. Saady, "Removal of sulfur compounds from real diesel fuel employing the encapsulated mesoporous material adsorbent Co/MCM-41 in a fixed-bed column," *Microporous and Mesoporous Materials*, vol. 341, article 112020, 2022.

[133] C. Sentorun-Shalaby, S. K. Saha, X. Ma, and C. Song, "Mesoporous-molecular-sieve-supported nickel sorbents for adsorptive desulfurization of commercial ultra-low-sulfur diesel fuel," *Applied Catalysis B: Environmental*, vol. 101, no. 3-4, pp. 718–726, 2011.

[134] C. L. Chuang, M. Fan, M. Xu et al., "Adsorption of arsenic(V) by activated carbon prepared from oat hulls," *Chemosphere*, vol. 61, no. 4, pp. 478–483, 2005.

[135] J. Zhu, Z. Lou, Y. Liu, R. Fu, S. A. Baig, and X. Xu, "Adsorption behavior and removal mechanism of arsenic on graphene modified by iron–manganese binary oxide (FeMnO x/RGO) from aqueous solutions," *RSC advances*, vol. 5, no. 83, pp. 67951–67961, 2015.

[136] M. Kragović, A. Daković, Ž. Sekulić et al., "Removal of lead from aqueous solutions by using the natural and Fe(III)-modified zeolite," *Applied Surface Science*, vol. 258, no. 8, pp. 3667–3673, 2012.

[137] W. Mozgawa and T. Bajda, "Spectroscopic study of heavy metals sorption on clinoptilolite," *Physics and Chemistry of Minerals*, vol. 31, no. 10, pp. 706–713, 2005.

[138] C. Liu, H. H. Ngo, and W. Guo, "Watermelon rind: agro-waste or superior biosorbent?," *Applied Biochemistry and Biotechnology*, vol. 167, no. 6, pp. 1699–1715, 2012.

[139] R. Leyva-Ramos, M. S. Berber Mendoza, J. Mendoza Barrón, and A. Aragón Piña, "Intercambio iónico de Pb (II) en solución acuosa sobre clinoptilolita modificada por intercambio catiónico," *Revista de la Sociedad Química de México*, vol. 48, no. 2, pp. 130–136, 2004.

[140] Y. Lv, B. Ma, Y. Liu, C. Wang, and Y. Chen, "Adsorption behavior and mechanism of mixed heavy metal ions by zeolite adsorbent prepared from lithium leach residue," *Microporous and Mesoporous Materials*, vol. 329, article 111553, 2022.

[141] C. G. Lee, J. W. Jeon, M. J. Hwang et al., "Lead and copper removal from aqueous solutions using carbon foam derived from phenol resin," *Chemosphere*, vol. 130, pp. 59–65, 2015.

[142] S. Jangkorn, S. Youngme, and P. Praipipat, "Comparative lead adsorptions in synthetic wastewater by synthesized zeolite A of recycled industrial wastes from sugar factory and power plant," *Heliyon*, vol. 8, no. 4, p. e09323, 2022.

[143] L. Rozumová, O. Životský, J. Seidlerová, O. Motyka, I. Šafařík, and M. Šafaříková, "Magnetically modified peanut husks as an effective sorbent of heavy metals," *Journal of Environmental Chemical Engineering*, vol. 4, no. 1, pp. 549–555, 2016.

[144] Y. H. Li, S. Wang, Z. Luan, J. Ding, C. Xu, and D. Wu, "Adsorption of cadmium(II) from aqueous solution by surface oxidized carbon nanotubes," *Carbon*, vol. 41, no. 5, pp. 1057–1062, 2003.

[145] M. R. Panuccio, A. Sorgonà, M. Rizzo, and G. Cacco, "Cadmium adsorption on vermiculite, zeolite and pumice: batch experimental studies," *Journal of Environmental Management*, vol. 90, no. 1, pp. 364–374, 2009.

[146] H. Javadian, F. Ghorbani, H. A. Tayebi, and S. H. Asl, "Study of the adsorption of cd (II) from aqueous solution using zeolite-based geopolymer, synthesized from coal fly ash; kinetic, isotherm and thermodynamic studies," *Arabian Journal of Chemistry*, vol. 8, no. 6, pp. 837–849, 2015.

[147] G. Buema, N. Lupu, H. Chiriac et al., "Performance assessment of five adsorbents based on fly ash for removal of cadmium ions," *Journal of Molecular Liquids*, vol. 333, article 115932, 2021.

[148] D. Mohan and K. P. Singh, "Single-and multi-component adsorption of cadmium and zinc using activated carbon derived from bagasse an agricultural waste," *Water Research*, vol. 36, no. 9, pp. 2304–2318, 2002.

[149] F. Sardella, M. Gimenez, C. Navas, C. Morandi, C. Deiana, and K. Sapag, "Conversion of viticultural industry wastes into activated carbons for removal of lead and cadmium," *Journal of Environmental Chemical Engineering*, vol. 3, no. 1, pp. 253–260, 2015.

[150] D. Aggarwal, M. Goyal, and R. C. Bansal, "Adsorption of chromium by activated carbon from aqueous solution," *Carbon*, vol. 37, no. 12, pp. 1989–1997, 1999.

[151] P. Maneechakr and S. Mongkollertlop, "Investigation on adsorption behaviors of heavy metal ions (Cd^{2+}, Cr^{3+}, Hg^{2+} and Pb^{2+}) through low- cost/active manganese dioxide-modified magnetic biochar derived from palm kernel cake

residue," *Journal of Environmental Chemical Engineering*, vol. 8, no. 6, article 104467, 2020.

[152] A. S. K. Kumar, S. J. Jiang, and W. L. Tseng, "Effective adsorption of chromium (VI)/Cr (III) from aqueous solution using ionic liquid functionalized multiwalled carbon nanotubes as a super sorbent," *Journal of Materials Chemistry A*, vol. 3, no. 13, pp. 7044–7057, 2015.

[153] X. Liu, Y. Zhang, Y. Liu, and T.'. Zhang, "Green method to synthesize magnetic zeolite/chitosan composites and adsorption of hexavalent chromium from aqueous solutions," *International Journal of Biological Macromolecules*, vol. 194, pp. 746–754, 2022.

[154] M. Liu, T. Wen, X. Wu et al., "Synthesis of porous Fe_3O_4 hollow microspheres/graphene oxide composite for Cr (VI) removal," *Dalton Transactions*, vol. 42, no. 41, pp. 14710–14717, 2013.

[155] A. S. K. Kumar, S. S. Kakan, and N. Rajesh, "A novel amine impregnated graphene oxide adsorbent for the removal of hexavalent chromium," *Chemical Engineering Journal*, vol. 230, pp. 328–337, 2013.

[156] L. Zheng, Z. Dang, X. Yi, and H. Zhang, "Equilibrium and kinetic studies of adsorption of Cd(II) from aqueous solution using modified corn stalk," *Journal of Hazardous Materials*, vol. 176, no. 1-3, pp. 650–656, 2010.